FOR FURTHER TRAN

AIR FORCE INSTITUTE OF TECHNOLOGY

AIR UNIVERSITY
UNITED STATES AIR FORCE

D D C

JUN 20 1978

E
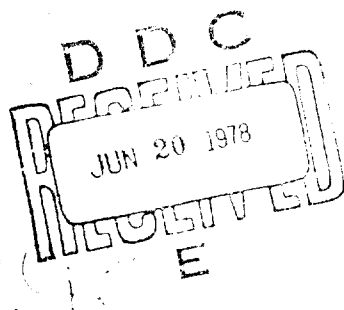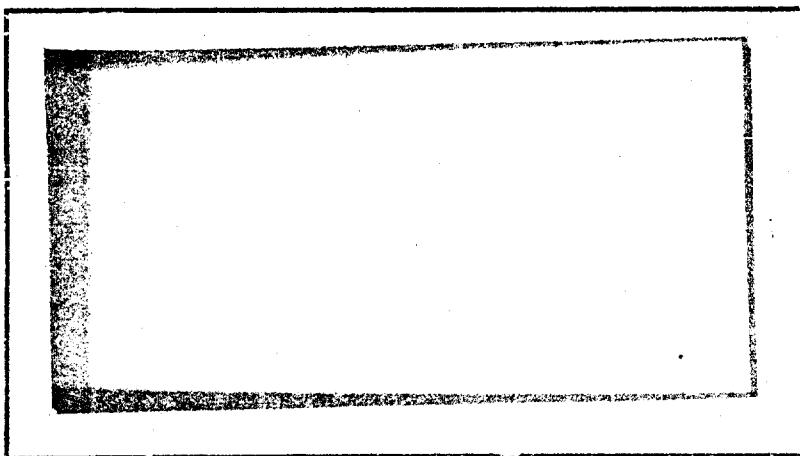
SCHOOL OF ENGINEERING
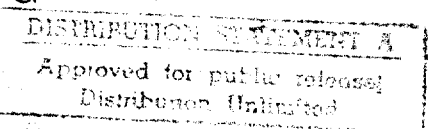
WRIGHT-PATTERSON AIR FORCE BASE, OHIO

18 06 13 080

①

OPTIMAL TERRAIN FOLLOWING CONTROLLER

FOR AN

OPTIMIZED SPLINE REFERENCE PATH

⑥

THESIS

AFIT/GA/EE/77-3   Ronald T. Kelly
                   Capt   USAF

Master's Thesis,

Dec 77

D D C

JUN 20 1978

E

Approved for public release; distribution unlimited.

OPTIMAL TERRAIN FOLLOWING CONTROLLER FOR

AN OPTIMIZED SPLINE REFERENCE PATH

THESIS

Presented to the Faculty of the School of Engineering

of the Air Force Institute of Technology

Air University

in Partial Fulfillment of the

Requirements for the Degree of

Master of Science

ACCESSION for		
NTIS	White Section	☒
DOC	Buff Section	[ ]
UNANNOUNCED		[ ]
JUSTIFICATION		
BY		
DISTRIBUTION/AVAILABILITY CODES		
Dist.	AVAIL. and/or SPECIAL	
A		

by

Ronald T. Kelly, B.S.

Capt   USAF

Graduate Astronautical Engineering

December 1977

Preface

This thesis is an extension of the previous work accomplished by Major James E. Funk, ASD/XRHA, Wright-Patterson AFB, Ohio. In his dissertation, the cubic spline reference paths for terrain following flight were not tracked by an optimal feedback controller. It was Major Funk who suggested I design an optimal controller for the cubic spline reference path.

I wish to thank my advisor, Major Funk, and my sponsor, Mr. Michael Breza, for their assistance during the preparation of this thesis. They both had set the foundation for this design study and had derived many of the basic relationships needed for the controller.

I also express my deep gratitude to my wife, Pam, for withstanding many lonely hours while I worked on completing this report. And I thank her for typing this thesis.

<div align="right">Ronald T. Kelly</div>

Contents

Contents

List of Figures

List of Figures

List of Figures

Abstract

This thesis presents the design of a proposed terrain following flight controller capable of tracking a cubic spline reference path. The controller tracks only the longitudinal motion; however, it provides both thrust and elevator control.

The controller is based on a nonlinear reference model constructed from an optimized spline path. The spline path altitude and associated derivatives are computed. The longitudinal equations of motion are linearized about the reference trajectory and a truth model of actual aircraft motion is developed. Deviations from the nonlinear reference trajectory to the actual provide a linear system. Optimal control theory is used to solve the resulting linear regulator problem. The feedback gains are calculated from the steady-state Ricatti matrix equation. The two system controls are updated using these feedback gains.

Results show the feedback controller to be stable and capable of tracking the cubic spline reference path. The performance index weighting matrices can be adjusted to improve the controller. The resulting controller can provide both good path control and engine control to improve vehicle survivability, engine life and fuel consumption.

OPTIMAL TERRAIN FOLLOWING CONTROLLER FOR

AN OPTIMIZED SPLINE REFERENCE PATH

I. Introduction

Low altitude high-speed flight has become a necessity
to increase penetration probability and survivability of
strategic bomber aircraft. This has resulted in emphasis
being placed on the terrain following mission profile.
And in recent years, the terrain following field has
broadened to include strategic cruise missile systems and
tactical helicopters. This broadening has been accompanied
by the incorporation of all the best features of modern
technology.

Current Problem

The terrain following mission creates severe demands
on the propulsion system of an aircraft. These demands
take the form of large and frequent fluctuations in the
thrust control system that result in shorter engine life
and increased fuel consumption. The operation of the
F-111 aircraft during the last ten years bears out this
problem. Maintenance reports conclude that the terrain
following mission adversely affects both engine wear and
fuel consumption (Ref 2:4).

Modern control theory has progressed to the point
where effective computational techniques can definitely
minimize the disadvantages of terrain following flight.

1

Also, the state of the art in on-board computer systems
is such that the required real-time calculations are
achievable. The coupling of control theory with better
computation leads to development of better terrain follow-
ing systems which reduce engine wear by minimizing throttle
control motion.

Currently, the problem which exists is the design of
a system that optimally controls all the aspects of ter-
rain following flight. The controller must be capable
of maintaining minimum deviations from a designated
reference path while providing reduced engine wear and
decreased fuel consumption.

Background

The fundamental problem in terrain following flight
is determining the commands to the control system which
achieve a desired flight path. Extensive research has
been addressed to this one area alone. As a result, many
methods and computer algorithms have been developed to
fly the terrain following mission. These methods encom-
pass the flight-path angle controllers and the path
controllers. Each of these categories contains a hierarchy
of improved development featuring an optimal tracking
system at the top. Accounting for the present state of
the art, these optimal trackers provide accurate naviga-
tion with minimal deviation from the nominal flight path.
But none of these optimal methods adequately accounts for
the thrust control problem.

2

The thrust control problem has not been considered
because present terrain following control laws essentially
decouple vertical flight path control from speed control.
These control laws assume a constant speed as the aircraft
contours the terrain. It can be seen that maintaining a
constant speed throughout a wide variety of flight-path
angles will certainly cause large engine thrust fluctua-
tions. Even though present terrain following control laws
use the constant speed assumption, recent tests have
shown that the overall system still performs well when
the actual speed varies slightly (Ref 8:1). Apparently,
the control system is fairly insensitive to reasonable
speed variations. Therefore, a control law which allows
reasonable velocity deviations from nominal will produce
lessened throttle adjustment. The best way to achieve
this is to incorporate throttle control, speed of the
aircraft, and vertical flight path so that these all will
interrelate and be optimally controlled. This allows a
trade-off between speed variation and thrust fluctuation
while flying the desired reference flight path.

The Boeing Aerospace Company attacked the problem
using an optimal integrated terrain following system
(Ref 8). This optimal system controls both altitude and
speed while accounting for vertical acceleration con-
straints and available engine thrust. Boeing's design
minimizes a quadratic performance index which includes
the following characteristics:

(a) Altitude deviation from desired flight path

(b) Speed deviation from set speed

(c) Vertical acceleration command

(d) Throttle command

The adjoint differential equations for the feed forward tracking signals are processed in accelerated reverse time to generate the current terrain following commands. Once each second a new desired path is computed.

The results of the Boeing integrated model show that the throttle motion was reduced dramatically when compared to current terrain following control systems. Only half the excess fuel used by previous controllers was consumed on the same profile. The Boeing simulation maintained aircraft speed closer to the set speed and minimized the altitude standard deviation over a typical flight profile. The only adverse effect was that the aircraft vertical acceleration was increased, and this resulted in a degradation of ride quality. This is quite important for pilot comfort, and can be improved by adjusting the acceleration limits within the system model (Ref 8:46).

Overall, the Boeing design provides the basis for an optimal controller, but it does not provide for an optimized reference path. The optimized cubic spline reference path generator developed by Major James E. Funk achieves this goal. The optimized spline path incorporates clearance, slope and acceleration constraints in the optimization problem, and generates a cubic spline as

4

a reference path. This path has continuous first and second derivatives. Each solution to this optimization problem results in a smooth reference path which follows the terrain as closely as possible. Because this smooth path contains continuous first and second derivatives, an aircraft should easily be able to fly this path. So, if an optimal controller can be found which uses the optimized cubic spline generated path as a reference, the aircraft controllability will be maximized and the thrust control problem will be minimized.

Scope

The object of this thesis is to demonstrate the feasibility of an optimal controller which attempts to fly an optimized spline reference path. This report uses optimal control theory with special emphasis on optimal linear state feedback control.

The optimal controller is based on deviations from a nonlinear reference model. The feedback gains are computed for a system linearized about the reference model based on a quadratic performance index somewhat different from the one used by Boeing. The linearized equations are also used to estimate the proper value for the weighting matrices. The feedback gains will be used in the nonlinear simulation of aircraft motion to evaluate the optimal controller. Performance of the controller will be evaluated under varying conditions.

This study will investigate the optimal controller

5

for aircraft only. The aircraft data used in the simulation is typical of a medium-sized advanced fighter.

Assumptions

In order to simplify the very complex nature of the nonlinear equations of motion certain assumptions must be made. These are as follows:

(a) A reliable set of discrete terrain data points is available

(b) Aircraft motion is restricted to the vertical plane

(c) No pilot will be in the control loop, so automatic operation is assumed

(d) The variations in speed of sound, mass of the aircraft, and atmospheric density are negligible

(e) The center-of-gravity of the aircraft does not change during flight

(f) Perfect navigation data on the state of the aircraft is used (Ref 9:102)

II. Description of the Control System

To adequately begin discussion of the proposed terrain following controller, it is necessary to describe the basic components of the entire system. The remainder of this report will further explain the mechanization of each of the components. Figures 1a, 1b and 1c illustrate the control system.

First of all, it will be assumed that the aircraft is equipped with some modern sensor device which provides accurate range and altitude data for the terrain. This can be achieved by using a forward looking radar, a laser ranger or even a map-matching terrain data processor. The method of data acquisition is not important to this report, as long as good terrain data is available.

Next, this reliable range and altitude data is fed into the reference path generator. It is here that the reference flight path is constructed in the range domain. The range domain is chosen in order to more directly fit and control the flight path with respect to the terrain. It is important that the reference path is constructed to inherently satisfy any acceleration, flight-path angle, and clearance constraints imposed upon the vehicle. Linear variations about this reference trajectory will be considered later, and any limits encountered by these perturbations will destroy the linear behavior and degrade the controller performance. The reference path description consists of the path altitude, h, and its first four

7
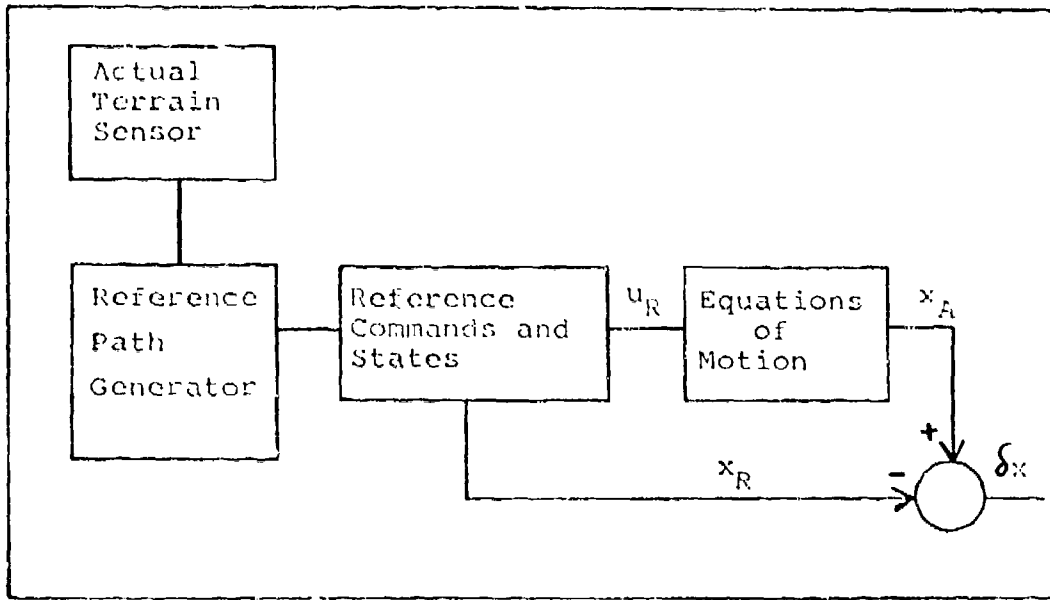
Figure 1a. Open Loop Controller
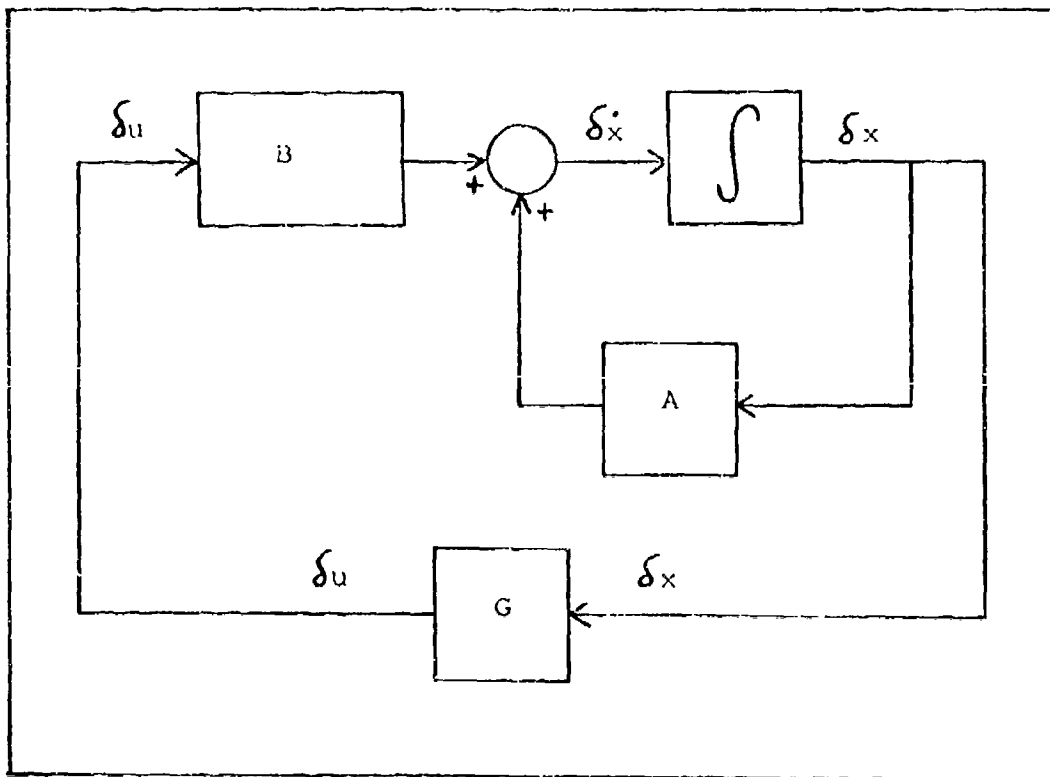
Figure 1b. Error Controller

8
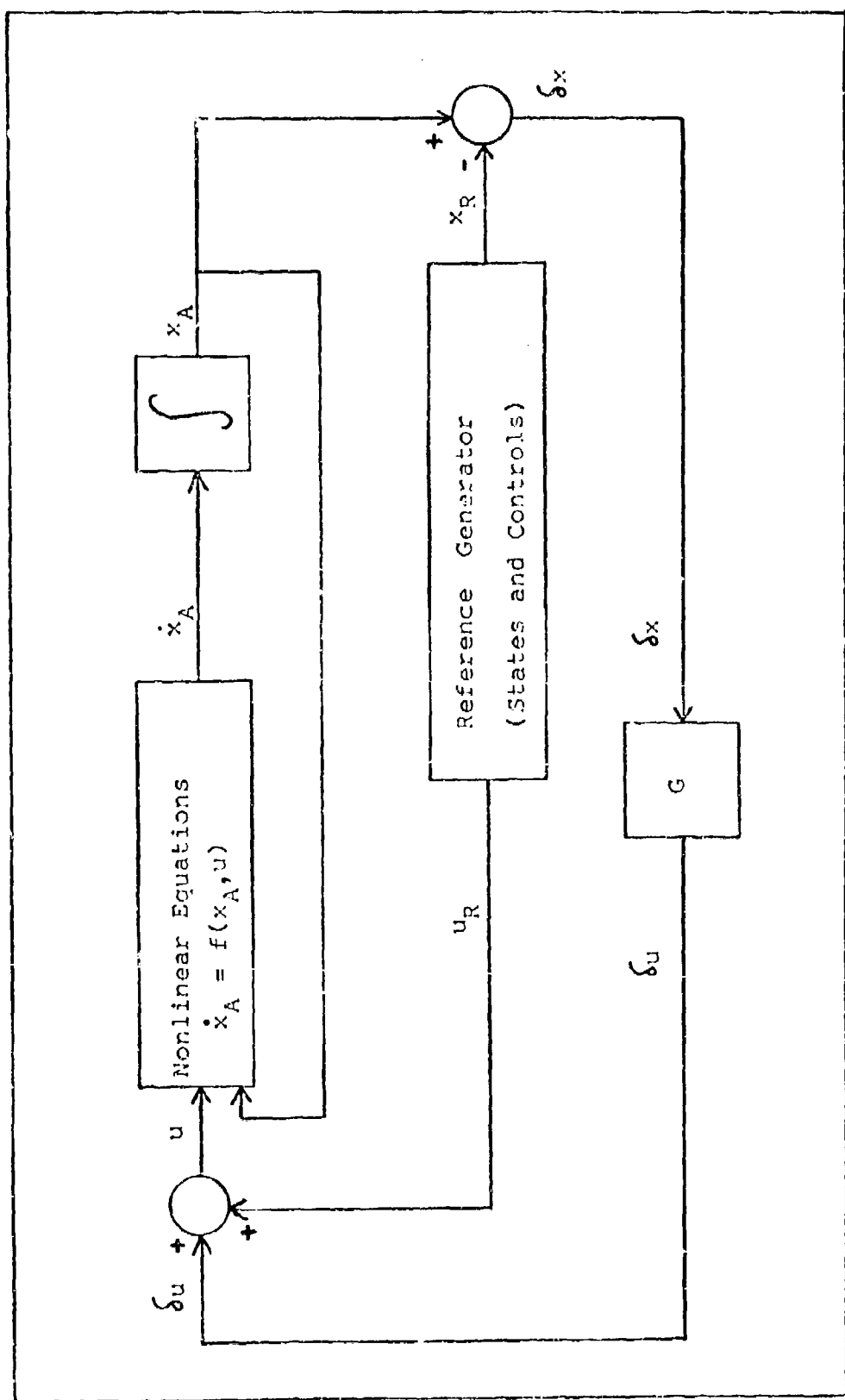
Figure 1c. Proposed Optimal Terrain Following Controller

(spatial) derivatives with respect to range, h', h'', h''' and h^{iv}.

These spatial variables are used for all subsequent reference model computations to obtain the desired velocity, the reference control and the reference state variables. The velocity generator computes the desired velocity, V_d, along the reference path by using some form of energy management criteria. This desired velocity can account for the operational speed limits of the aircraft as well as the desired average groundspeed to successfully meet the check point times on the low level mission. The desired velocity and all the calculations of flight path are used to compute the complete set of reference states, x_R. These reference states are then used to compute the estimates of the reference controls, u_R, needed to produce such reference states. This completes the generation of all the necessary reference data to begin the simulation sequence.

The nonlinear aircraft differential equations are processed to simulate the actual state representation for the aircraft. These states are denoted as x_A. In reality the true aircraft states cannot be determined exactly. The actual states would be estimated from a number of measurements. This would involve filtering techniques and various sensing devices. However, in this thesis the control system errors, rather than the sensor errors, are of major interest; therefore, it is assumed that

integration of the differential equations of motion provides the exact states of aircraft motion and estimation theory is excluded.

A comparison is next made between the actual aircraft state, x_A, and the corresponding reference states, x_R, to compute the state deviation δx. These state deviations are kept small by the selection of the proper feedback gain matrix, G. More explanation will be given to this topic in Chapter III.

The feedback gain matrix, G, is calculated through optimal control laws (explained in Chapter III) and the Ricatti equation. The matrix, G, can be maintained as a constant for most of the terrain following missions to be flown. This is consistent with the system design since the state deviations are small, and variables such as atmospheric density and aircraft mass are assumed constant for the terrain following profiles to be used in this thesis (Gain scheduling is possible for extended missions).

Once the feedback gain matrix, G, is calculated a feedback control signal, δu, can be computed. This signal, δu, is achieved by multiplying the feedback gain matrix, G, with the state deviation, δx, in the following manner (Ref 4:151 and 13:194)

$$\delta u = G \, \delta x \tag{1}$$

The feedback control signal, δu, can then be added to the previously computed reference control, u_R, to provide the

11

actual control, u. This control, u, provides the necessary commands to the aircraft engine and aerodynamic control system to maintain the aircraft close to the reference trajectory.

With the computation of the actual control, u, the system loop in Fig. 1c is essentially completed. New data is sensed ahead of the aircraft, new reference parameters are computed, and new controls are activated in a sequence of data frames. This, basically, is the overall operation of the proposed terrain following controller. The remainder of the thesis describes the components of this controller and their interactions in more detail. The results of the simulation are also discussed.

III. Optimization of the Linear Controller

The entire approach to the optimal terrain following
controller is based on the methods of modern control
theory. This theory forms the foundation for the prelimi-
nary study of the proposed controller.

The Regulator Problem

The function of a state regulator is to maintain the
states of a system within an acceptable deviation from
the zero reference condition by using required control.
This is the type of feedback controller to be designed
and used in this project.

The system, in this case, consists of the deviations
from a time-variant reference model and thus is a linear-
ized system.

$$\delta \dot{x}(t) = A \, \delta x(t) + B \, \delta u(t) \qquad (2)$$

In Eq (2)

$\delta x(t)$ is the nx1 vector of perturbed states

$\delta u(t)$ is the mx1 vector of perturbed controls

A   is the nxn dynamics matrix

B   is the nxm control distribution matrix

Both A and B are time-variant, but they are assumed to
vary slowly to allow quasi-steady state solution of the
controller gains.

The reference conditions are generated by the path
generator, the state generator and the control generator
as described in Chapter II. In addition, the reference

13

velocity is calculated continuously along the flight path. For this thesis the initial reference velocity is 647.3 ft/sec which is Mach .58 at sea level conditions. This initial reference velocity can be used as a nominal flight condition. Since variations in flight condition are not large, the aerodynamic stability derivatives are assumed constant in the region of interest while the reference states change with time.

The perturbation state vector, $\delta\underline{x}$, can be written as

$$\delta\underline{x} = \underline{x}_A - \underline{x}_R \tag{3}$$

where

$\underline{x}_A$ is the actual state vector

and

$\underline{x}_R$ is the reference state vector

and the perturbation control vector, $\delta\underline{u}$, can be written similarly as

$$\delta\underline{u} = \underline{u} - \underline{u}_R \tag{4}$$

where

$\underline{u}$ is the actual control vector

and

$\underline{u}_R$ is the reference control vector

The two quantities, $\delta\underline{x}$ and $\delta\underline{u}$, represent the deviations from their respective reference conditions. And these are the values which will be regulated by the optimal feedback

14

controller developed for this thesis.

For the optimal terrain following regulator an appropriate cost function must be designed. The most convenient and workable form is the quadratic which weights both the state and the control deviations from a reference condition. The conventional quadratic cost function will be (Ref 4:149)

$$J = \frac{1}{2} \int_{0}^{T \to \infty} \left(\delta \underline{x}^T P \delta \underline{x} + \delta \underline{u}^T R \delta \underline{u} \right) dt \qquad (5)$$

This form shows that the state deviations and the control deviations are directly regulated depending on the form of the weighting matrices P and R. But for this controller, not all of the state deviations are to be regulated directly. Instead, an output deviation, δy, will be regulated directly. As will be seen later, this merely represents a particular choice of the P matrix.

The output is defined as

$$\delta \underline{y} = C \delta \underline{x} \qquad (6)$$

where C is the transformation matrix. Using the output deviation, δy, the cost function can be written as

$$J = \frac{1}{2} \int_{0}^{T \to \infty} \left(\delta \underline{y}^T Q \delta \underline{y} + \delta \underline{u}^T R \delta \underline{u} \right) dt \qquad (7)$$

The selection of the two weighting matrices, Q and R, will be described at the end of this chapter.

The transpose of the output vector, δy, is

15

$$\delta\underline{y}^T = \left(C\,\delta\underline{x} \right)^T = \delta\underline{x}^T C^T \tag{8}$$

Substitution of Eq (8) and Eq (6) into Eq (7) produces the revised cost function

$$J = \frac{1}{2} \int_0^{T\to\infty} \left(\delta\underline{x}^T C^T Q C\,\delta\underline{x} + \delta\underline{u}^T R\,\delta\underline{u} \right) dt \tag{9}$$

Comparison of Eqs (5) and (9) shows that they are equivalent if $P = C^T Q C$. The cost function in Eq (9) is also in the form to use the Ricatti equation to determine the Ricatti gain matrix, S.

The Ricatti Equation

The solution to the regulator problem requires solution of the Ricatti equation (Ref 4:167). For simplicity, it is assumed that the dynamics matrix, A, and the control distribution matrix, B, are constant matrices. This assumption is not strictly true and results in a sub-optimal set of gains. In the cost function of Eq (9) the weighting matrix, R, is assumed constant as is the product matrix, $C^T Q C$. With these assumptions the steady state Ricatti equation is written in the form

$$\dot{S} = 0 = -SA - A^T S + SBR^{-1}B^T S - C^T QC \tag{10}$$

This equation above implies that the Ricatti gain matrix, S, is constant for the optimal terrain following regulator (Ref 4:167). If terrain following occurred for prolonged

16

periods, the gains could be scheduled for varying flight
conditions. The solution of Eq (10) is accomplished by
using the OPTSYS program described in Appendix E.

Linear State Feedback

When solving for the feedback gain matrix, G, from
Chapter II, the linear control law of Eq (1) can be
written in vector form as

$$\delta \underline{u} = G \delta \underline{x} \tag{11}$$

This value for $\delta \underline{u}$ can be substituted in Eq (2) to obtain

$$\delta \underline{\dot{x}} = A \delta \underline{x} + BG \delta \underline{x} \tag{12}$$

Factoring out $\delta \underline{x}$ from Eq (12) yields

$$\delta \underline{\dot{x}} = \left(A + BG \right) \delta \underline{x} \tag{13}$$

The term, A+BG, is known as the closed loop dynamics
matrix because this term incorporates the feedback gain
matrix, G, as seen in Fig. 1.

A connection may now be made between the feedback
gain matrix, G, and the Ricatti gain matrix, S. Since S
is the steady-state Ricatti gain matrix it can be shown
that (Ref 4:167 and 13:221)

$$G = -R^{-1} B^{T} S \tag{14}$$

and the steady-state linear control law of Eq (11)
becomes

$$\delta \underline{u} = -R^{-1}B^{T}S\, \delta \underline{x} \tag{15}$$

This equation above forms the basic control law for the linear regulator problem considered in this thesis. It is Eq (15) which updates the control for the terrain following regulator according to

$$\underline{u} = \underline{u}_{R} + \delta \underline{u} \tag{16}$$

Determination of Q and R Matrices

There is no one standard method for determining the exact components of the Q and R weighting matrices for any given problem. It requires some iterations and educated guesswork to determine the best overall weights. Both the Q and R matrices will be used in diagonal form only. This is done because normally only the main diagonal elements are significant (Ref 4:149 and 10:33). The Q matrix weights each deviation in the four output variables and the R matrix weights the deviation in the two control variables.

The method of Bryson and Ho (Ref 4:149) can be used to obtain working values for the diagonal elements of both Q and R. This method utilizes the setting of maximum acceptable values on each element of the output deviation vector, $\delta \underline{y}$, and the control deviation vector, $\delta \underline{u}$. Corresponding elements of the weighting matrices can then be used in the cost function, J. The equations for deter-

18

mining the diagonal element weights are

$$1/Q_{ii} = \text{the maximum acceptable value of } \left[\delta y_i\right]^2 \quad (17)$$

and

$$1/R_{ii} = \text{the maximum acceptable value of } \left[\delta u_i\right]^2 \quad (18)$$

It should be noted that these two equations will produce a "first guess" set of diagonal elements which can be adjusted to obtain reasonable performance for the cost function. Once these weighting matrices have been established the resulting Ricatti gain matrix, S, is automatically fixed according to the Ricatti equation, Eq (10). This matrix, S, in turn, directly affects the overall value of the feedback gain matrix, G, as seen in Eq (14). Therefore, any change in the diagonal elements of either Q or R will create multiple changes in the subsequent gain matrices of the system.

The reason Bryson and Ho equations can be considered a "first guess" estimate is that certain selected Q and R diagonal elements may result in control values that are not realizable. In this fashion the Q and R matrices must be judiciously adjusted to obtain good performance without adversely affecting the flying qualities or the realizable control deviations.

If the diagonal elements of Q are increased the controller tends to become stronger and restrict the system deviations closer to zero. This can also be

achieved by decreasing the element values of R. A
stronger terrain following regulator will result in a
decrease in the response time of the overall system. But
this is usually accomplished with a corresponding increase
in peak overshoot. So these tradeoffs must be considered
when designing the best values for the diagonal elements
of the Q and R weighting matrices.

IV. The State Variables and Equations of Motion

The purpose of this chapter will be to denote the variables comprising the state vector and the control vector used in this thesis. Additionally, this chapter will describe the linearized equations of motion. A full development of the equations of motion will not be presented here, but the reader is directed to References 6, 7, 12, 14 and 16 if a fuller explanation is needed.

Only the longitudinal equations of motion will be used in this controller design since the longitudinal dynamics are the most important in a terrain following flight profile. The flight regime will be restricted to the x-z plane of motion as seen in Fig. 2. Lateral control is usually termed terrain avoidance and is beyond the scope of this thesis. Omission of the lateral equations of motion will not degrade the controller design nor provide inaccurate results. And because of near-
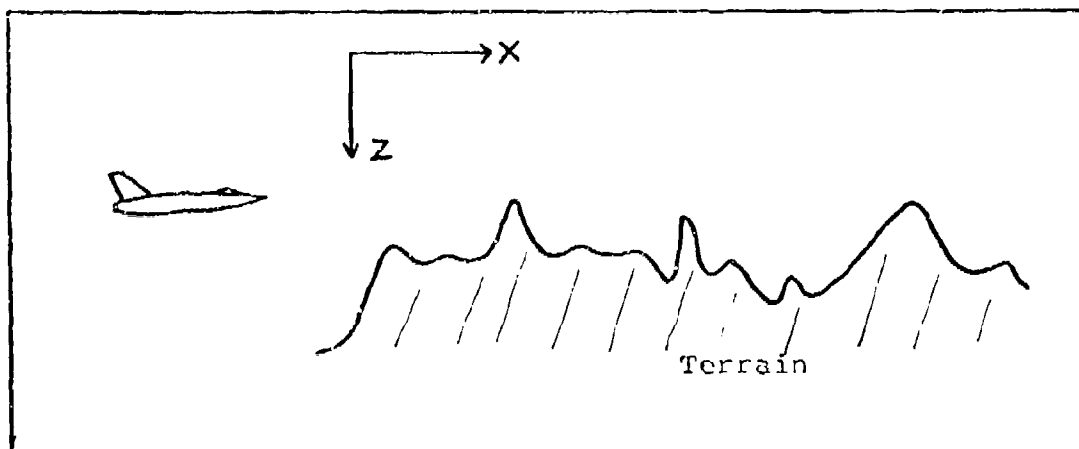
Figure 2. Two Dimensional Terrain Following Profile

21

symmetry of the aircraft the longitudinal equations of
motion may be separated from the lateral equations of
motion (Ref 17:218).
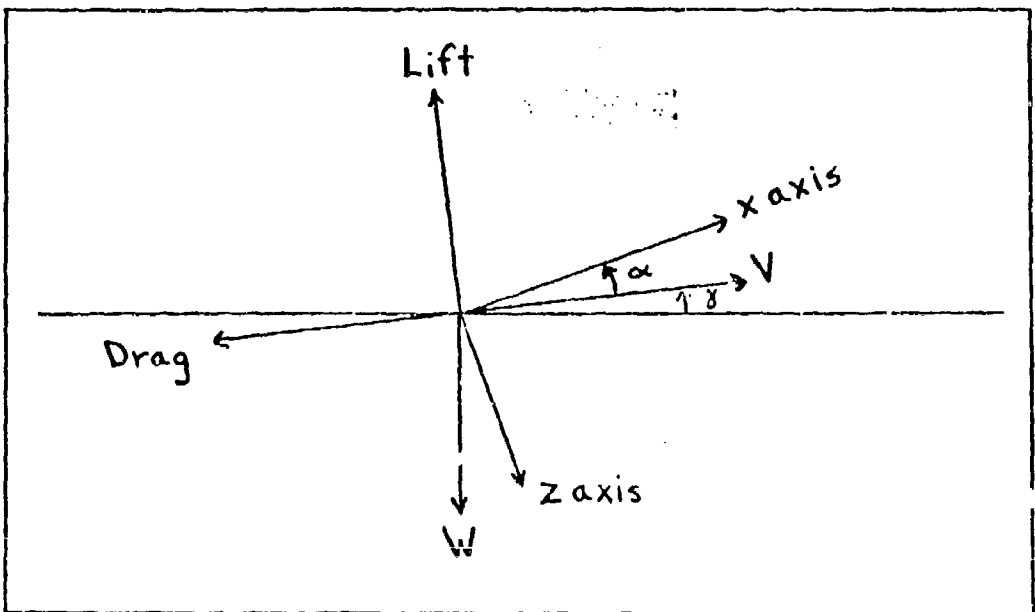
Figure 3. Axis System

Assumptions and Coordinate Axis

While developing the longitudinal equations of motion
the aircraft is assumed to be a rigid body. The variation
of the pitch angle, $\delta\Theta$, is assumed small so that

$$\cos \delta\Theta = 1$$

and

$$\sin \delta\Theta = \delta\Theta$$

And the forward velocity, V, is approximated by

$$V = \sqrt{U^2 + \omega^2} \approx U$$

The coordinate axes to be used will be a set of
stability axes that is fixed with respect to the reference
trajectory velocity vector. The relation to the x-z
body axes is shown in Fig. 3.

State Variables

For the design of this terrain following controller
there are seven state variables chosen to represent the
states of the system. These are

U	the longitudinal forward velocity
w	the normal velocity
q	the pitch rate
θ	the pitch angle
δ	the elevator deflection angle
Δ	the thrust
h	the altitude

These seven state variables will be used throughout this
thesis and will be collectively designated as the vector
$\underline{x}$.

Two of the state variables will be directly control-
led in this design project. These two command values
are the controls

δ_c the commanded elevator deflection angle

Δ_c the commanded thrust

and can be denoted as the control vector $\underline{u}$.

Perturbation Theory

For the purpose of designing the tracking controller,
the nonlinear longitudinal equations can be linearized
about a particular reference trajectory and the motion
described in terms of the variations in seven state
variables. This is illustrated in Fig. 4.
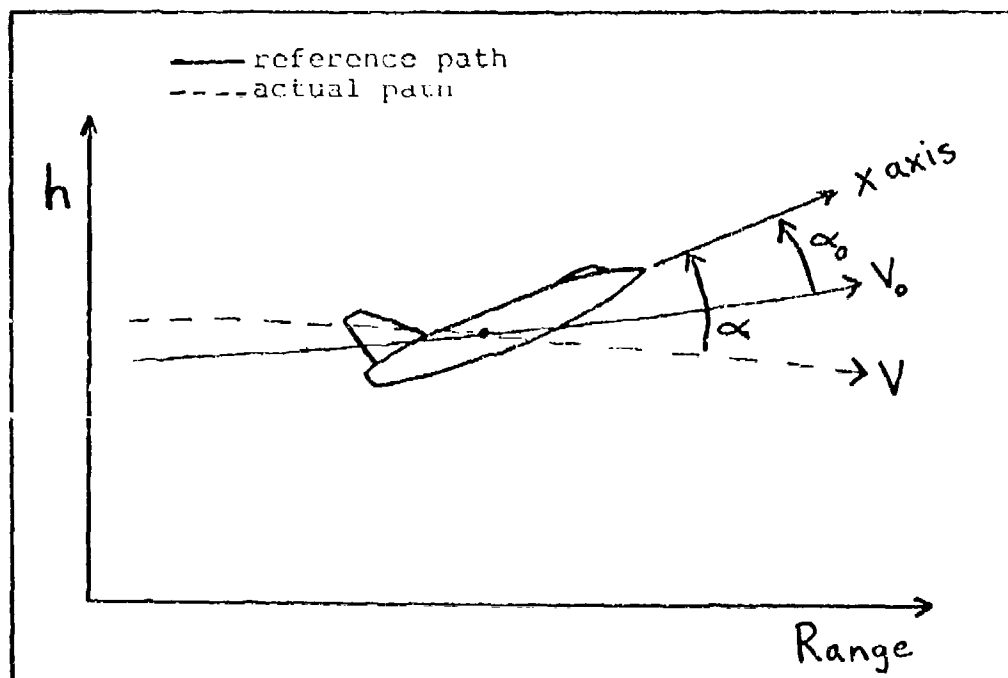
Figure 4. Perturbation about a Reference Trajectory

The use of small-disturbance theory can be used to pro-
duce the linearized perturbation equations of motion
(Ref 7:120). All the perturbation quantities and their
respective derivatives are assumed small so their squares
and products are negligible when compared to the first-
order linearization terms. A linearized perturbation in
angle of attack, α , is illustrated in Fig. 5.

$$\gamma = 0$$

$$\Delta\alpha$$

$$\alpha_0$$

$$\alpha = \alpha_0 + \Delta\alpha$$
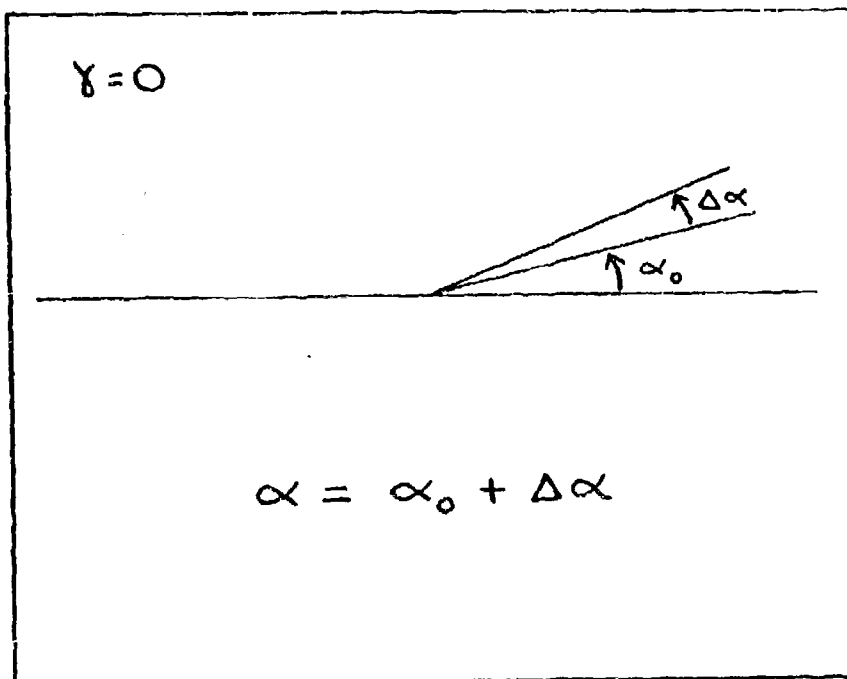
Figure 5. Linear Perturbation in Angle of
Attack

Linearized Perturbation Equations

The linearized perturbation equations for each of
the seven state variables can now be written using dimen-

25

sional stability derivatives. These dimensional stability derivatives are explained in Appendix B.

The fact that the equations are linearized about an arbitrary trajectory, rather than straight and level flight as is frequently done, means that the coefficients in the linearized equations would depend on the reference trajectory states. This implies that the coefficients would vary with time. In order to develop a controller with constant gains the coefficients must be constant. The assumption required for this is that the reference flight path angle, γ_R, and angle of attack, α_R, are small enough that their products with a perturbation state can be considered of second order. In this way the perturbation equations reduce to the usual form. Therefore, for the purpose of this study the usual linearization about straight and level flight was considered accurate enough to use for the linear perturbation model.

For the perturbation in longitudinal velocity, U:

$$\delta \dot{U} = X_U \, \delta U + X_w \, \delta w + X_q \, \delta q - g \, \delta\theta + X_\delta \, \delta\delta + X_\Delta \, \delta\Delta \tag{19}$$

For the perturbation in normal velocity, w:

$$\delta \dot{w} = Z_U \, \delta U + Z_w \, \delta w + \left(U_0 + Z_q\right)\delta q + Z_\delta \, \delta\delta + Z_\Delta \, \delta\Delta \tag{20}$$

where U_0 is the nominal forward velocity. For the perturbation in pitch rate, q:

$$\delta \dot{q} = M_U \, \delta U + M_w \, \delta w + M_q \, \delta q + M_\delta \, \delta\delta \tag{21}$$

26

For the perturbation in pitch angle, Θ :

$$\delta\dot{\Theta} = \delta q \tag{22}$$

For the perturbation in elevator deflection angle, δ :

$$\delta\dot{\delta} = -\frac{1}{\tau_e}\left(\delta\delta - \delta\delta_c\right) \tag{23}$$

where τ_e is the time constant associated with the elevator control, δ, and $\delta\delta_c$ is the elevator control command based on the feedback of perturbation states.

For the perturbation in thrust, Δ :

$$\delta\dot{\Delta} = -\frac{1}{\tau_p}\left(\delta\Delta - \delta\Delta_c\right) \tag{24}$$

where τ_p is the time constant associated with the thrust control, Δ, and Δ_c is the perturbation thrust command.

For the perturbation in altitude, h:

$$\delta\dot{h} = -\delta w + V_0\,\delta\Theta \tag{25}$$

These equations above, Eq (19) – Eq (25), constitute the longitudinal perturbation equations of motion in dimensional derivative form. These equations can be rewritten in the matrix form of the linear differential equation as

$$\delta\underline{\dot{x}} = A\,\delta\underline{x} + B\,\delta\underline{u} \tag{26}$$

where A is the open loop dynamics matrix. Gathering Eq (19) through Eq (25) into matrix form results in:

27

$$A = \begin{bmatrix} X_v & X_w & X_q & -g & X_\delta & X_\Delta & 0 \\ Z_v & Z_w & V_0 + Z_q & 0 & Z_\delta & Z_\Delta & 0 \\ M_v & M_w & M_q & 0 & M_\delta & 0 & 0 \\ 0 & 0 & 1 & 0 & 0 & 0 & 0 \\ 0 & 0 & 0 & 0 & -\tfrac{1}{\tau_e} & 0 & 0 \\ 0 & 0 & 0 & 0 & 0 & -\tfrac{1}{\tau_p} & 0 \\ 0 & -1 & 0 & V_0 & 0 & 0 & 0 \end{bmatrix} \qquad (27)$$

Forcing Function

The two aircraft control commands, δ_c and Δ_c, act as forcing functions for the linearized system of equations. This forcing function consists of a control distribution matrix, B, multiplied by the control command vector. The matrix B takes the form of:

$$
B = \begin{bmatrix} O & O \\ O & O \\ O & O \\ O & O \\ 1/\tau_e & O \\ O & 1/\tau_p \\ O & O \end{bmatrix} \tag{28}
$$

The commanded controls must also be written in the perturbation form as

$$
\delta \underline{u} = \begin{bmatrix} \delta \delta_c \\ \delta \Delta_c \end{bmatrix} \tag{29}
$$

This completely describes the terms in perturbation equation (26) which is identical to Eq (2) in Chapter III.

V. Cubic Spline Reference Path

This chapter discusses the main points regarding the generation of the optimized reference flight path. It is this reference path which the optimal terrain following controller is designed to follow as closely as possible. All of the information in this chapter originates in Reference 7 since the reference path generation is the essence of Major Funk's doctoral dissertation. As a result, this chapter will not detail the reference path generation, but will highlight those main ideas of importance to the design of an optimal terrain following controller.

Cubic Splines

A cubic spline function consists of a sequence of cubic polynomial segments which together form a continuous function having continuous first and second derivatives (Ref 1:54). Mathematical spline functions are ideally suited to digital trajectory computation. They provide smooth continuous curves that can be specified uniquely by a discrete set of parameters.

A cubic polynomial can be denoted as

$$ y(x) = y_i + A_i \left(\frac{x - x_i}{\Delta x} \right) + B_i \left(\frac{x - x_i}{\Delta x} \right)^2 + C_i \left(\frac{x - x_i}{\Delta x} \right)^3 \quad (30) $$

for $i = 1, 2, \ldots, n-1$

where $\Delta x = x_{i+1} - x_i$

A typical cubic spline function is shown in Fig. 6.
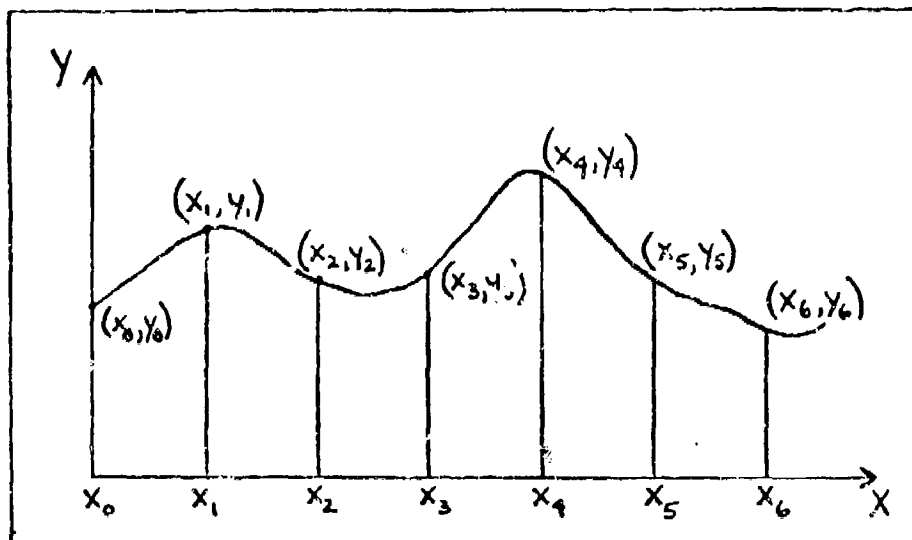
Figure 6. Cubic Spline Function

The function points (x_i, y_i) are called knots.

The first and second derivatives can be obtained by differentiating Eq (30). For the interior knots (x_2 through x_5 in Fig . 6) the first and second derivatives must be identical for each adjoining interval. This means the derivatives at knot (x_2, y_2) must be the same for x_1 to x_2 and for interval x_2 to x_3. This insures continuity. Therefore, the three unknowns for each segment, A_i, B_i, and C_i, can be computed by enforcing the continuity conditions at each interior point and by specifying the slope at each endpoint. In this manner a

31

unique cubic spline function can be constructed to represent the given data as a smooth, continuous function.

For a terrain following profile it is important to let the knots coincide with the terrain data. This procedure insures that the cubic function passes through each of the data points.

Terrain Data and Clearance Curve

The sampled terrain data is defined in the range domain rather than the time domain. This is ideal for a terrain following flight profile since terrain elevation is naturally described as a function of range rather than time. Therefore, Fig. 6 can represent the known terrain data if the ordinate becomes terrain elevation and the abscissa is range. This is illustrated in Fig. 7.
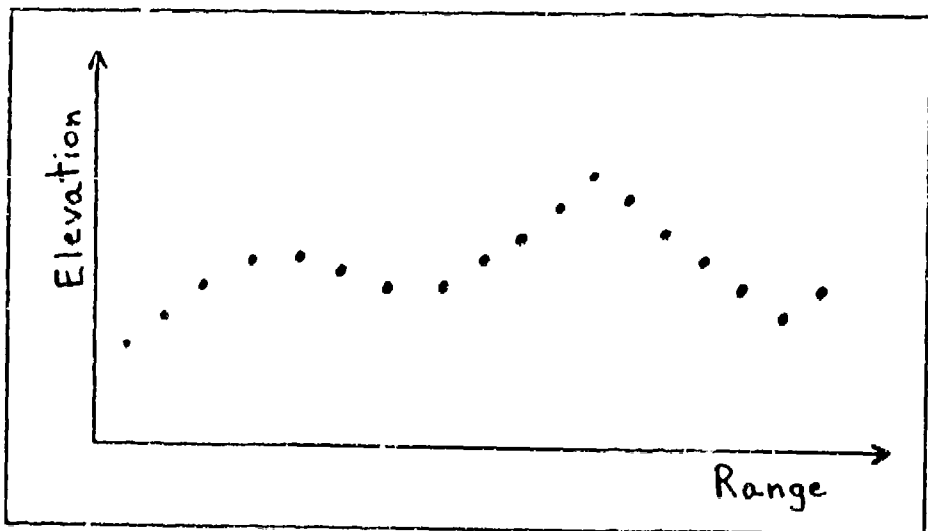
Figure 7. Sampled Terrain Data

The reference path generation begins with the input
of sampled terrain data. These data points consist of
the elevation of the terrain at specified range intervals.
For instance, the elevation (in feet) is specified for
each 2000 feet of range along the flight profile. The
reference path generator algorithm normalizes the raw
data and constructs a cubic spline function which passes
through the given set of terrain points. This is called
the terrain curve. Next, the minimum amount of clearance
above the terrain curve is specified. This designated
clearance is used for determination of the cubic spline
clearance curve. Both the terrain curve and the clearance
curve are shown in Fig. 8 below.
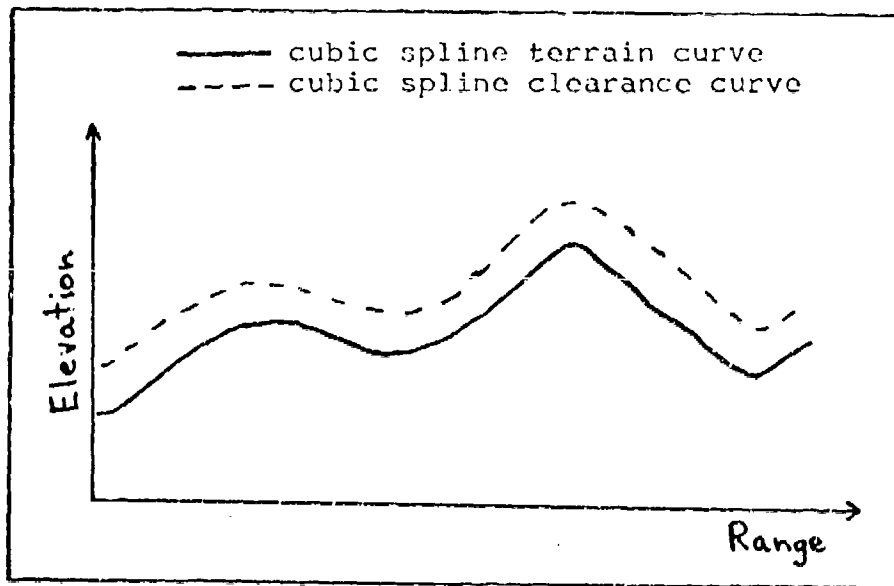
Figure 8. Terrain and Clearance Curves

The altitude along the cubic spline clearance curve is designated h, which is a function of range. Since the clearance curve is processed as a cubic spline path, h will represent a cubic spline function. The slope of the clearance curve, h', is defined as the first derivative of h with respect to range (spatial derivative) and designated as either h' or s.

$$h' = \frac{dh}{dR} = s \tag{31}$$

The second spatial derivative is

$$h'' = \frac{d^2h}{dR^2} = k \tag{32}$$

where h'' or k is called the curvature.
And the third spatial derivative is

$$h''' = \frac{d^3h}{dR^3} = p \tag{33}$$

where p or h''' is called the kink. As mentioned in the previous section on cubic spline functions, the variables h, s and k are continuous and p is piecewise continuous.

The Reference Path Optimal Control Problem

The cubic spline clearance curve can be considered a minimum clearance curve over the terrain. It would be extremely difficult, if not impossible, for a manned aircraft to track this minimum clearance curve efficiently within the aircraft performance limitations. Therefore,

the cubic spline clearance curve must be optimized by minimizing a performance index using optimal control theory. For this optimal control problem it is possible to specify certain constraints on k, s and p so that the limits of the aircraft are not exceeded and the aircraft does not descend below the minimum clearance curve. The performance index minimizes the deviation from the clearance curve while enforcing the specified constraints along the curve.

The reference path optimization problem is solved subject to the following inequality constraints along the entire range (Ref 9:35)

$$s_{min} \leq s \leq s_{max}$$

$$k_{min} \leq k \leq k_{max}$$

$$p_{min} \leq p \leq p_{max}$$

The limits on k are determined from the normal acceleration limits and the nominal aircraft speed by the following equation

$$k = \frac{a_{N_{max}}}{V_0^2} \tag{34}$$

This equation is accurate as long as the slope, s, is small. The k limits tend to occur at the tops of peaks and near the bottoms of valleys where the slope is nearly zero. So Eq (34) is a good approximation.

Framing of the Optimal Control Problem

It would be very impractical to solve an extremely large optimal control problem for the entire terrain following flight profile. As a result, the optimal control problem must be broken into specified segments called frames (Ref 9:44).

The framing procedure is illustrated in Fig. 9 where there is no overlap between frames. For Frame 1, essen-
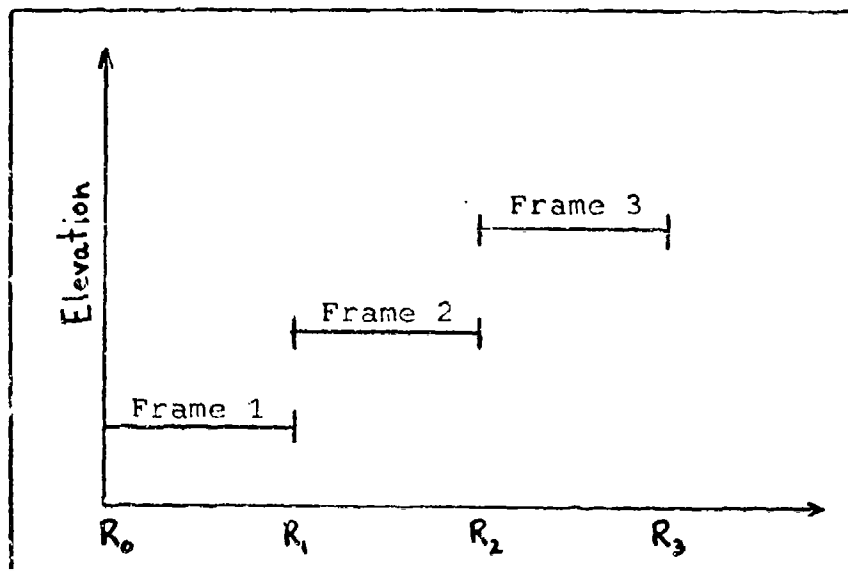
Figure 9. Framing with no Overlap

tially an optimal control problem is performed over the range interval R_0 to R_1. At range R_1 a new optimal control problem is begun for the range interval for R_1 to R_2. This framing procedure with no overlap would work well if the input terrain data were perfect. But because of radar shadowing the present state of the art

36

does not allow the accurate solution with no frame over-
lap. There must be an overlap between frames so that as
updated terrain data ahead of the aircraft is sensed, a
new optimization problem can be solved to update the
previously computed flight path signals. The computer
algorithm developed by Major Funk optimizes the entire
reference flight path by overlapping frames as can be
seen in Fig. 10. This overlap allows for a continuous
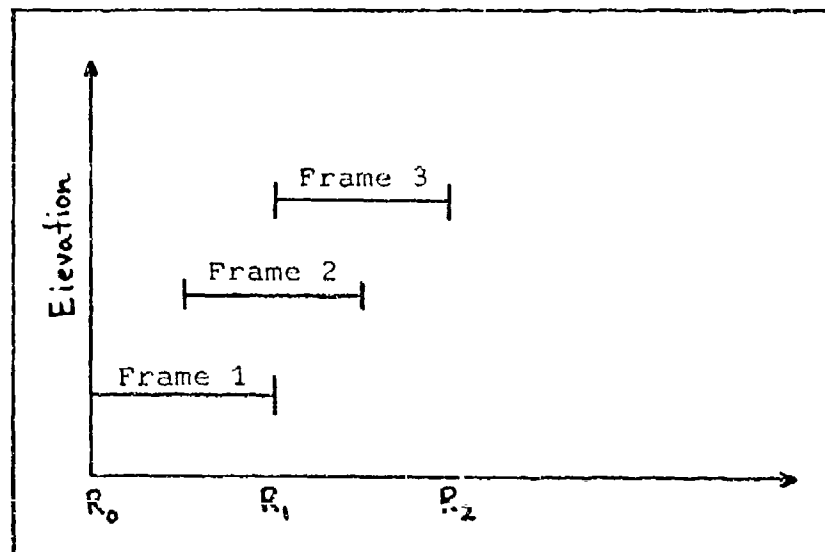
Figure 10. One-half Frame Overlap

update of the reference flight path as new terrain
information is detected.

Within each frame a certain number of control points
are specified. These control points correspond to the

points at which the constraints on h, s, k and p must be satisfied. As the number of control points per frame increases, the computation time also increases. So there is a tradeoff between using a large number of control points which forces the reference path to more closely follow the terrain, and using a small number of control points which reduces the computation time and the control rate.

In addition to the control points, there are numerous other parameters which must be specified in each frame of the solution to the optimization problem. These various parameters will not be described here since they are listed in Reference 9, page 54. But the availability of such a variety of parameters permits the flexibility in the generation of the optimized cubic spline reference path for various aircraft and missions. This reference path generator can account for almost all the practical constraints for any type of flight vehicle on varying terrain following profiles.

Output of the Reference Path Generator

The output of the reference path generator consists of the optimized cubic spline reference path as shown in Fig. 11. It can be seen that the reference path does not coincide with the minimum clearance curve. The main reason for the difference between the two curves is that the reference path must satisfy all the specified con-
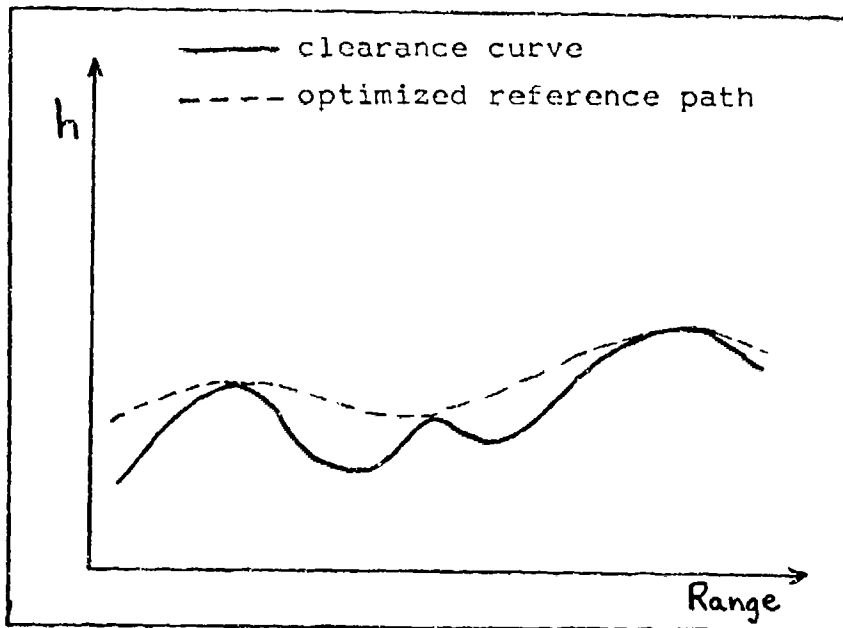
Figure 11. Optimized Reference Path

straints along the flight profile. Generally some por-
tions of the clearance curve will have excessive curva-
tures or slopes which would exceed the acceleration and
flight-path angle constraints. Whenever the clearance
curve satisfies the specified constraints the two curves
will coincide.

The actual numerical output of the reference path
generator consists of the optimized path altitude, h, and
its slope, h', at each discrete increment of range, R_i.
This path data is then input to an interpolation routine
which reconstructs the full cubic spline using a direct
slope determination technique (Ref 9:61 and 18:54). This

cubic spline interpolation routine calculates the follow-
ing parameters at any desired range along the flight
profile:

    (a) h - altitude

    (b) h' - slope

    (c) h'' - curvature

    (d) h''' - kink

These four quantities can then be used in the nonlinear
equations which represent the cubic spline terrain
following controller outlined in Chapter VI.

Some Important Relationships

    Before describing the nonlinear reference model it
will be helpful to show some important relationships
between the time and spatial derivatives along the
reference path. Since altitude, h, is really a function
of range it can be written

$$h = h\big(R(t)\big) \tag{35}$$

where range, R, is a function of time. From Fig. 12 the
time derivatives of range and altitude are shown in rela-
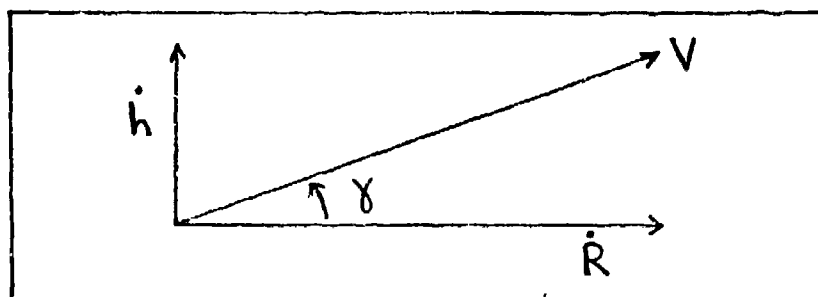
Figure 12. Relationship between $\dot{h}$, $\dot{R}$ and V

40

tion to the velocity, V. These relationships can be written as (Ref 11:306 and 15:64)

$$\dot{h} = V \sin \gamma \qquad (36)$$

and

$$\dot{R} = V \cos \gamma \qquad (37)$$

But $\dot{h}$ can also be written as

$$\dot{h} = \frac{dh}{dR} \frac{dR}{dt} = h' V \cos \gamma \qquad (38)$$

which is another representation of the same quantity in Eq (36).

The time derivative of slope, h', can be computed from

$$\dot{h}' = \frac{d(h')}{dt} = \frac{dh'}{dR} \frac{dR}{dt} = h'' V \cos \gamma \qquad (39)$$

These equations above will be important for the nonlinear equations of Chapter VI.

41

VI. Nonlinear Reference Model

This chapter describes the nonlinear equations used
to construct the reference model for the optimal terrain
following controller. In Chapter IV the linear model with
the perturbation equations was presented. But the non-
linear equations must be used in the design simulation
since the nonlinear model more accurately represents the
actual aircraft flight regime. The nonlinear response
and stability characteristics provide a more realistic
controller operation. The purpose of this chapter is to
show the development of the equations leading to the
reference model state vector, $\underline{x}_R$, and the truth model,
$\underline{x}_A$. Then these two state vectors can be used to obtain
the commanded control vector, $\underline{u}$, necessary for tracking
the cubic spline reference path. A partial block diagram
of this development is shown in Fig. 13 below.
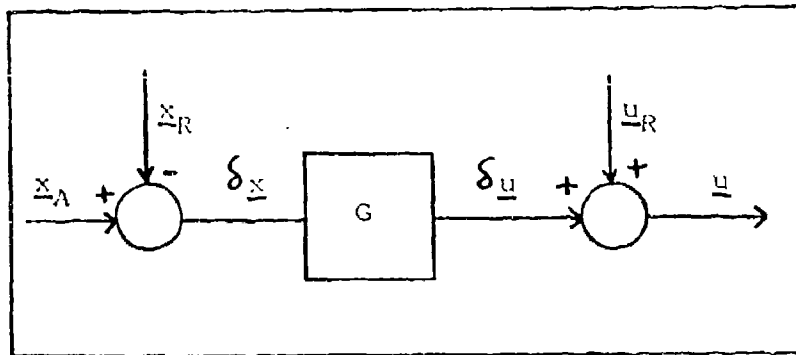
Figure 13. Computation of Commanded Control, $\underline{u}$

An attempt has been made to organize this chapter sequen-

tially through the equation derivations in the order in which they are required.

Reference Path Generation

The cubic spline reference path generator described in Chapter V provides the necessary altitude and derivative data to construct the optimized flight path. The path generator calculates the following reference quantities in the range domain:

(a) h_d - reference altitude

(b) h_d' - slope

(c) h_d'' - curvature

(d) h_d''' - kink

where the subscript, d, denotes desired or reference quantity. These four quantities are essential to the computation of many other reference conditions.

Reference Velocity Generator

To correlate time and spatial relations along the flight path, velocity must be known. The desired velocity along the reference path could be computed from energy management considerations once the path is known. For simplicity, a constant energy assumption is made here. If the terrain is not too severe and the vehicle kinetic energy is large, this is a reasonable assumption. This allows an interchange of kinetic and potential energy with a corresponding reduction in throttle activity over that required for constant speed flight.

43

Starting with the initial velocity, V_o, and the initial altitude, h_o, the total specific energy of the system is computed by summing the specific potential and kinetic energies as

$$E_o = \frac{1}{2} V_o^2 + g h_o \qquad (40)$$

The cubic spline reference path generator provides a value for desired altitude, h_d, at any point along range. So the desired velocity, V_d, may be computed by rearranging the constant energy equation

$$V_d = \sqrt{2 \left(E_o - g h_d \right)} \qquad (41)$$

This is the equation for calculating desired or reference velocity along range.

Reference Flight Path Angle and First Time Derivative

The flight path angle, γ, can be computed using the trigonometric relation shown in Fig. 14.
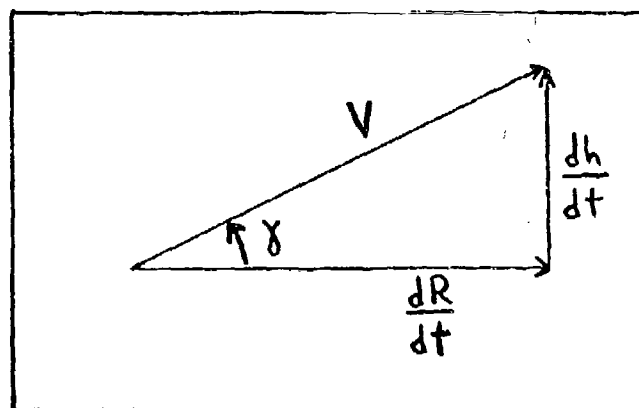
Figure 14. Flight Path Angle, γ

44

The angle, γ, is related by

$$\tan \gamma = \frac{dh}{dR} = h'$$

(42)

Since h'_d is computed by the reference path generator the desired flight path angle, γ_d, is

$$\gamma_d = \tan^{-1} h'_d$$

(43)

The first derivative of γ with respect to time can be written

$$\dot{\gamma} = \frac{d\gamma}{dR} \frac{dR}{dt} = \frac{d\gamma}{dt}$$

(44)

where

$$\frac{d\gamma}{dR} = \gamma'$$

and

$$\frac{dR}{dt} = \dot{R} = V \cos \gamma$$

An expression for γ' can be derived by taking the spatial derivative of both sides of Eq (42). This results in

$$\gamma' = h'' \cos^2 \gamma$$

(45)

Substituting Eq (37) and Eq (45) into Eq (44) yields the expression for the first time derivative of γ_d

$$\dot{\gamma}_d = h''_d V_d \cos^3 \gamma_d$$

(46)

Time Derivatives of Velocity

Now that the flight path angle and its first time derivative are derived, it is possible to obtain the first and second time derivatives of desired velocity.

The assumption of constant energy implies

$$\dot{E}_o = 0 \tag{47}$$

After differentiation of both sides of Eq (40) the first time derivative of velocity becomes

$$\dot{V}_d = \frac{-g\dot{h}_d}{V_d} \tag{48}$$

From Eq (38) in Chapter V the $\dot{h}_d$ term may be replaced by

$$\dot{h}_d = h'_d V_d \cos \gamma_d \tag{49}$$

Substituting Eq (49) into Eq (48) yields

$$\dot{V}_d = -g h'_d \cos \gamma_d \tag{50}$$

This is the expression for the first time derivative of desired velocity. The second time derivative can be derived in a similar manner.

If Eq (42) is written with the reference subscript, d, it becomes

$$h'_d = \tan \gamma_d \tag{51}$$

This form of h_d' permits substitution in Eq (50) to produce

$$\dot{V}_d = -g \sin \gamma_d \qquad (52)$$

Differentiating both sides of Eq (52) with respect to time results in

$$\ddot{V}_d = -g \cos \gamma_d \; \dot{\gamma}_d \qquad (53)$$

Substitution of Eq (46) for $\dot{\gamma}_d$ shows that

$$\ddot{V}_d = -g \, h_d'' \, V_d \cos^4 \gamma_d \qquad (54)$$

Eq (54) is the equation for the second time derivative of desired velocity and this equation will be used in the nonlinear model.

Definition of K and its Derivatives

Since one important term reappears in many subsequent equations it is convenient to define the quantity, K, called the mathematical path curvature (it is inversely proportional to the instantaneous radius of curvature (Ref 9:149)).

$$K \triangleq h_d'' \cos^3 \gamma_d \qquad (55)$$

The first derivative of K with respect to range is

$$K' = h_d''' \cos^3 \gamma_d - 3 h_d'' \cos^2 \gamma_d \sin \gamma_d \; \gamma_d' \qquad (56)$$

47

Substitution of Eq (45) for γ'_d yields

$$K' = h'''_d \cos^3 \gamma_d - 3\left(h''\right)^2 \cos^4 \gamma_d \sin \gamma_d \qquad (57)$$

But Eq (57) can be written in terms of K as

$$K' = h'''_d \cos^3 \gamma_d - 3K^2 \sec^2 \gamma_d \sin \gamma_d \qquad (58)$$

Eq (58) is the expression for the spatial derivative of K. (In subsequent equation derivations the subscript, d, will be omitted, but it is still assumed that all quantities will be those desired for the reference model).

The time derivatives of K are now obtained from differentiation of Eq (55) with respect to time so that

$$\dot{K} = \frac{d(h'')}{dt} \cos^3 \gamma - 3 h'' \sin \gamma \cos^2 \gamma \, \dot{\gamma} \qquad (59)$$

But it can be seen that

$$\frac{d(h'')}{dt} = \frac{d(h'')}{dR} \frac{dR}{dt} \qquad (60)$$

which equals

$$\frac{d(h'')}{dt} = h''' V \cos \gamma \qquad (61)$$

If the $\dot{\gamma}$ equation, Eq (46), is written in terms of K it becomes

$$\dot{\gamma} = KV \qquad (62)$$

Substituting Eq (61) and Eq (62) into Eq (59) shows that the first time derivative of K is

$$\dot{K} = h''' V \cos^4 \gamma - 3 h'' K V \sin \gamma \cos^2 \gamma \qquad (63)$$

And this can be written more compactly as

$$\dot{K} = V \left(h''' \cos^4 \gamma - 3 h' K^2 \right) \qquad (64)$$

The second time derivative of K results from taking the derivative of both sides of Eq (64).

$$\ddot{K} = \dot{V} \left(h''' \cos^4 \gamma - 3 h' K^2 \right) + V \left(h^{iv} V \cos^5 \gamma - \right.$$

$$\left. 4 h''' \cos^3 \gamma \sin \gamma \dot{\gamma} - 3 h'' V \cos \gamma K^2 - 6 h' K \dot{K} \right) \qquad (65)$$

where $h^{iv} = 0$ for a cubic spline function.

After much manipulation and rearrangement of Eq (65) it can be rewritten in slightly shorter form as

$$\ddot{K} = \dot{K} \left(\frac{\dot{V}}{V} - 10 \gamma h' \right) + V^2 \left[h^{iv} \cos^5 \gamma - 3 K^3 \left(1 + 5 h'^2 \right) \right] \qquad (66)$$

Second Time Derivative of Flight Path Angle

With all the equations for K it is now possible to derive the second time derivative of the flight path angle. Differentiation of Eq (62) with respect to time is

$$\ddot{\gamma} = \dot{K} V + \dot{V} K \qquad (67)$$

Substitution of Eq (64) into Eq (67) produces

$$\ddot{\gamma} = V^2\left(h''' \cos^4 \gamma - 3h'K^2\right) + \dot{V}K \qquad (68)$$

This equation is the expression for the second time derivative of γ and is used later for computation of the angular rates for the nonlinear equations.

Forces in the Lift Direction

This section derives one important equation which will be used for other reference model computations. This equation results from the summation of all forces in the lift direction. From the forces shown in Fig. 15
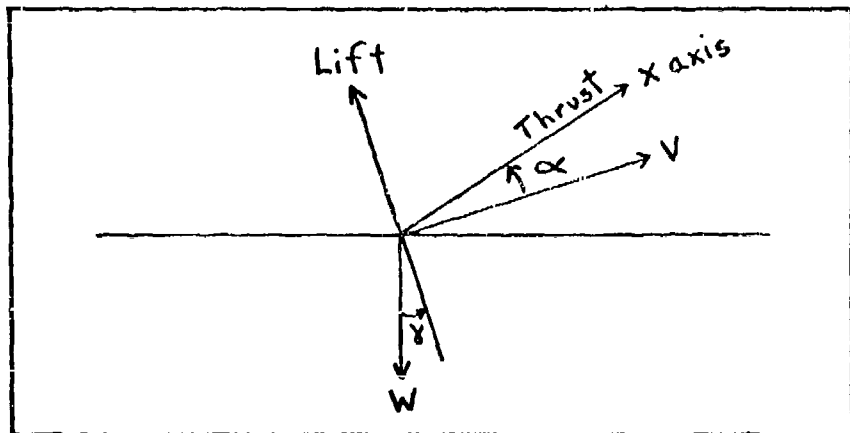
Figure 15. Forces in the Lift Direction

the force equation is

$$m\,a_N = L + T\sin\alpha - mg\cos\gamma \qquad (69)$$

where a_N is the acceleration in the lift direction.
This acceleration, a_N, is shown in Fig. 16 and can be
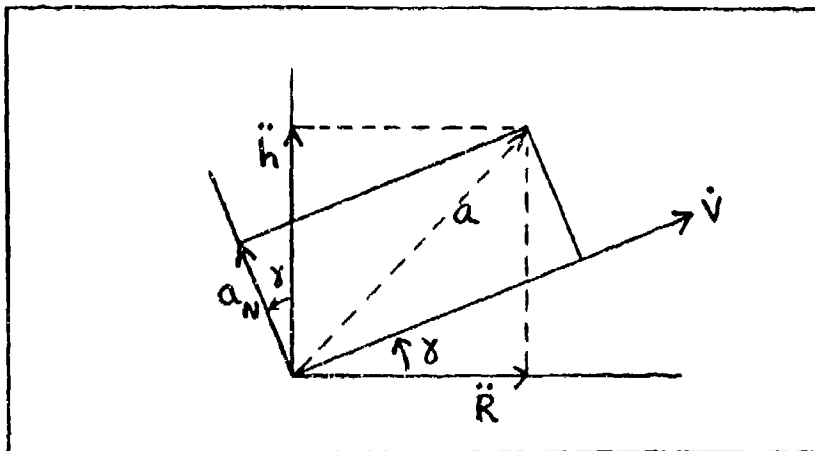
Figure 16. Acceleration in Lift Direction
(Ref 9:149)

written as

$$a_N = \ddot{h} \cos \gamma - \ddot{R} \sin \gamma \qquad (70)$$

The normal acceleration can also be written as

$$a_N = KV^2 = h'' V^2 \cos^3 \gamma \qquad (71)$$

since K is the inverse of the instantaneous radius of
curvature (Ref 9:151). The lift force, L, can be written

$$L = \bar{q} S C_L \qquad (72)$$

Both Eq (71) and Eq (72) can be substituted into Eq (69)
for the following equation

51

$$C_L + \frac{T}{\bar{q}S} \sin\alpha = \frac{m}{\bar{q}S}\left(KV^2 + g\cos\gamma\right) \qquad (73)$$

The lift coefficient, C_L, can be expressed as

$$C_L = C_{L_o} + C_{L_\alpha}\alpha + C_{L_\delta}\delta + C_{L_{\bar{M}}}\Delta\bar{M} \qquad (74)$$

where $\bar{M}$ denotes Mach number. Using the small angle approximation and substituting Eq (74) into Eq (73) yields

$$\left(C_{L_\alpha} + \frac{T}{\bar{q}S}\right)\alpha + C_{L_\delta}\delta = \frac{m}{\bar{q}S}\left(KV^2 + g\cos\gamma\right) -$$

$$C_{L_{\bar{M}}}\Delta\bar{M} - C_{L_o} \qquad (75)$$

Eq (75) is the first of two equations which will be solved as a simultaneous set later in this chapter.

Estimated Angle of Attack and Derivatives

In order to obtain an estimate of the angle of attack (call this α_E) the following conditions are set on Eq (75)

$$C_{L_\delta} = C_{L_{\bar{M}}} = C_{L_o} \approx 0$$

This is done so the resulting expression for the estimated angle of attack, α_E, can be used for computing the time derivatives of α needed in subsequent equations (the actual reference value for α is obtained later without assuming the zero conditions above). So, after the zero

52

conditions are set in Eq (75) the resulting expression for estimated angle of attack is

$$\alpha_E \cong \left(KV^2 + g\cos\gamma\right)\left[\frac{\bar{q}S}{m}C_{L_\alpha} + \frac{T}{m}\right]^{-1} \qquad (76)$$

At this point it is convenient to define a variable, C_A, as

$$C_A \overset{\triangle}{=} \left[\frac{\bar{q}S}{m}C_{L_\alpha} + \frac{T}{m}\right]^{-1} \qquad (77)$$

Using Eq (77) the expression for α_E becomes

$$\alpha_E \cong \left(KV^2 + g\cos\gamma\right)C_A \qquad (78)$$

Differentiation of Eq (78) with respect to time results in

$$\dot{\alpha}_E = \dot{C}_A\left(KV^2 + g\cos\gamma\right) + C_A\left(\dot{K}V^2 + 2KV\dot{V} - g\sin\gamma\,\dot{\gamma}\right) \qquad (79)$$

An expression for $\dot{C}_A$ is

$$\dot{C}_A = -\left[\frac{\bar{q}SC_{L_\alpha} + T}{m}\right]^{-2}\left(\frac{\dot{\bar{q}}SC_{L_\alpha}}{m}\right) \qquad (80)$$

which can be written

$$\dot{C}_A = \frac{-C_A^2 \rho V\dot{V}SC_{L_\alpha}}{m} \qquad (81)$$

Substituting Eq (81) into Eq (79) yields

53

$$\dot{\alpha}_E = \frac{-C_A^2 \rho V \dot{V} S C_{L_\alpha}}{m}\left(KV^2 + g\cos\gamma\right) + C_A\left(\dot{K}V^2 + 2KV\dot{V} - g\sin\gamma\,\dot{\gamma}\right) \quad (82)$$

But it can be seen from Eq (78) that

$$\frac{\alpha_E}{C_A} = KV^2 + g\cos\gamma \quad (83)$$

Therefore, after some substitution Eq (82) may be rewritten in terms of α_E as

$$\dot{\alpha}_E = \frac{-C_A \rho V \dot{V} S C_{L_\alpha}}{m}\alpha_E + C_A\left(\dot{K}V^2 + 2KV\dot{V} - g h' V K\cos\gamma\right) \quad (84)$$

After rearranging and factoring, $\dot{\alpha}_E$ takes the final form of

$$\dot{\alpha}_E = C_A V\left[\dot{K}V - g h' K\cos\gamma + \dot{V}\left(2K - \frac{\rho S C_{L_\alpha}}{m}\alpha_E\right)\right] \quad (85)$$

Eq (85) is now used to obtain the second derivative of α_E with respect to time. Initially this equation is

$$\ddot{\alpha}_E = \dot{C}_A V\left(\frac{\dot{\alpha}_E}{C_A V}\right) + C_A \dot{V}\left(\frac{\dot{\alpha}_E}{C_A V}\right) +$$

54

$$C_A V \left[\ddot{K}V + \dot{K}\dot{V} - g\dot{K}h'\cos\gamma - g K \dot{h}'\cos\gamma + \right.$$

$$g K h' \sin\gamma \dot{\gamma} + \ddot{V}\left(2K - \frac{\rho S C_{L\alpha}}{m}\alpha_E\right) +$$

$$\left. \dot{V}\left(2\dot{K} - \frac{\rho S C_{L\alpha}}{m}\dot{\alpha}_E\right)\right] \tag{86}$$

After factoring this equation can be written as

$$\ddot{\alpha}_E = \dot{\alpha}_E\left(\frac{\dot{V}}{V} + \frac{\ddot{V}}{\dot{V}} - \frac{4\bar{q}\,\dot{V} S C_{L\alpha}}{L\,mV}\right) +$$

$$C_A V^2 \left[\ddot{K} + \dot{K}\left(\frac{3\dot{V}}{V} - \frac{\ddot{V}}{\dot{V}}\right) + \right.$$

$$\left. \frac{g\cos\gamma\,K}{V}\left(h'\left(\frac{\ddot{V}}{\dot{V}} - \frac{\dot{K}}{K}\right) - \dot{\gamma}\right)\right] \tag{87}$$

Now that the time derivative equations, Eq (85) and Eq (87), are derived these quantities can be used in further development of the nonlinear equations. It must be recalled that these angle of attack derivatives were derived from an estimated angle of attack equation, Eq (76).

The Moment Equation

For an aircraft in flight the moment equation is

$$M_\gamma = I_\gamma \ddot{\Theta} \tag{88}$$

where
$$M_y = \bar{q} S \bar{c} C_m$$

and
$$\ddot{\Theta} = \dot{q}$$

Eq (88) can be rewritten as

$$C_m = \frac{I_y \dot{q}}{\bar{q} S \bar{c}} \tag{89}$$

But the pitching moment coefficient, C_m, can be expanded as

$$C_m = C_{m_0} + C_{m_\alpha} \alpha + C_{m_\delta} \delta + C_{m_{\bar{M}}} \Delta \bar{M} +$$

$$\frac{\bar{c}}{2 V_0} \left(C_{m_q} q \right) \tag{90}$$

Eq (90) can be substituted in Eq (89) to yield

$$C_{m_\alpha} \alpha + C_{m_\delta} \delta = \frac{I_y \dot{q}}{\bar{q} S \bar{c}} - \frac{\bar{c}}{2 V_0} \left(C_{m_q} q \right) -$$

$$C_{m_0} - C_{m_{\bar{M}}} \Delta \bar{M} \tag{91}$$

This equation, Eq (91), is the second of two equations forming a set of simultaneous equations which are used for computing elevator deflection, δ, and angle of attack, α. The first equation was Eq (75).

Reference States

With all the preliminary equation derivations completed, the seven reference state equations will be developed in this section. The seven reference states comprising the reference state vector are:

U_R reference velocity in the x-direction

w_R reference normal velocity in the z-direction

q_R reference pitch rate

Θ_R reference pitch angle

δ_R reference elevator deflection

Δ_R reference thrust (T_R is equation notation)

h_d reference or desired altitude

Reference Thrust. For computation of reference thrust the forces are summed along the velocity axis as shown in Fig. 17. The force equation is

$$m\dot{V} = T_R \cos\alpha - D - mg\sin\gamma \qquad (92)$$
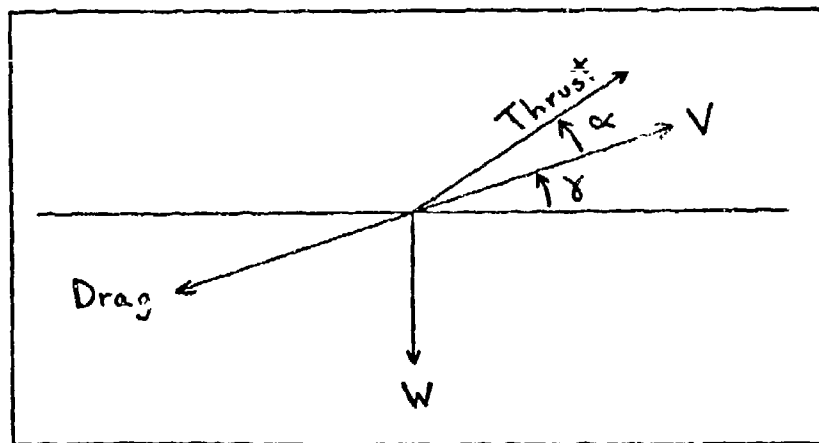
Figure 17. Forces in Velocity Direction

57

Solving for reference thrust

$$T_R = \frac{m\dot{V} + \bar{q}SC_D + mg\sin\gamma}{\cos\alpha} \tag{93}$$

which can be rewritten as

$$T_R = \sec\alpha\left(m\dot{V} + \bar{q}SC_D + mg\sin\gamma\right) \tag{94}$$

Eq (94) is the equation for reference thrust. The only available value for angle of attack, α, at this point, is α_E which is used in this equation. (In actual computation reference thrust is updated by using the reference angle of attack, α_R, which is derived in the next section).

Reference Elevator Deflection and Reference Angle of Attack. Since a value for reference thrust has been computed in Eq (94) it is now possible to solve the two simultaneous equations, Eq (75) and Eq (91). These two previous equations can be written in matrix form as

$$\begin{bmatrix} C_{L_\alpha} + \dfrac{T_R}{\bar{q}S} & C_{L_\delta} \\[2ex] C_{m_\alpha} & C_{m_\delta} \end{bmatrix} \begin{bmatrix} \alpha_R \\[2ex] \delta_R \end{bmatrix} = \begin{bmatrix} \dfrac{m}{\bar{q}S}\left(KV^2 + g\cos\gamma\right) - C_{L_{\bar{M}}}\Delta\bar{M} - C_{L_0} \\[2ex] \dfrac{I_y\dot{q}}{\bar{q}S\bar{c}} - \dfrac{\bar{c}}{2V_0}\left(C_{m_q}q\right) - C_{m_0} - C_{m_{\bar{M}}}\Delta M \end{bmatrix} \tag{95}$$

For conciseness, let

58

$$C_{L_\alpha}^* \triangleq C_{L_\alpha} + \frac{T_R}{\bar{q}S}$$

and let

$$\Delta CLD \triangleq \frac{m}{\bar{q}S}\left(KV^2 + g\cos\gamma\right) - C_{L_{\bar{M}}}\Delta\bar{M} - C_{L_0}$$

and

$$\Delta CMD \triangleq \frac{I_y q}{\bar{q}S\bar{c}} - \frac{\bar{c}}{2V_0}C_{m_q}q - C_{m_{\bar{M}}}\Delta\bar{M} - C_{m_0}$$

The values for q and $\dot{q}$ must be computed from values obtained from Eqs (46), (63), (85) and (87) such that

$$q = \dot{\gamma} + \dot{\alpha}_E$$

and

$$\dot{q} = \ddot{\gamma} + \ddot{\alpha}_E$$

Using Cramer's Rule, Eq (95) may be solved for the two reference states of δ_R and α_R. The final results are

$$\delta_R = \frac{C_{L_\alpha}^* \Delta CMD - C_{m_\alpha}\Delta CLD}{C_{L_\alpha}^* C_{m_\delta} - C_{m_\alpha}C_{L_\delta}} \tag{96}$$

and

$$\alpha_R = \frac{C_{m_\delta} \Delta CLD - C_{L_\delta} \Delta CMD}{C_{L_\alpha}^* C_{m_\delta} - C_{m_\alpha} C_{L_\delta}} \tag{97}$$

Now that these two reference angles have been derived, the remainder of the reference states follow.

Reference Velocities in x and z Directions. From the relationship shown in Fig. 18 the following equations
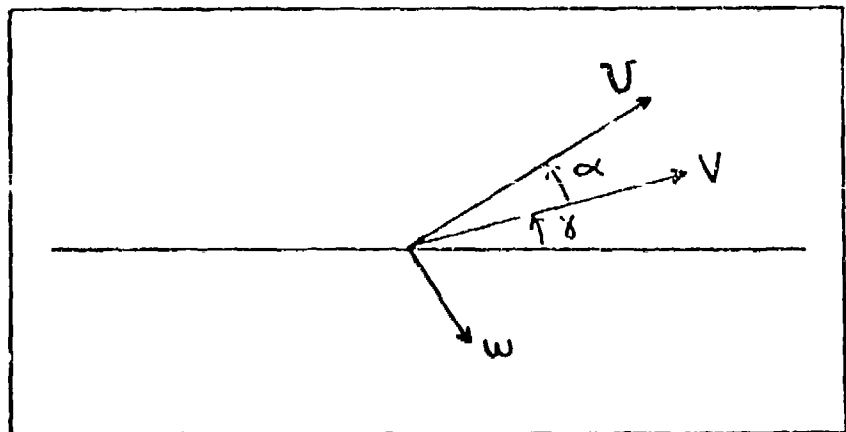
Figure 18. Velocities in x and z directions

result

$$U_R = V \cos \alpha_R \tag{98}$$

and

$$w_R = V \sin \alpha_R \tag{99}$$

60

<u>Reference Pitch Rate</u>. The reference pitch rate is derived from the basic definition of

$$q = \dot{\alpha} + \dot{\gamma} \qquad (100)$$

Using the reference angles

$$q_R = \dot{\alpha}_R + \dot{\gamma}_d \qquad (101)$$

where $\dot{\alpha}_R$ comes from Eq (35) with α_E replaced by α_R and $\dot{\gamma}_d$ comes from Eq (46).

<u>Reference Pitch Angle</u>. The reference pitch angle, Θ, is derived also from the basic definition

$$\Theta_R = \alpha_R + \gamma_d \qquad (102)$$

where α_R is from Eq (97) and γ_d is from Eq (43).

<u>Reference Altitude</u>. The reference or desired altitude, h_d, is computed in the reference path generator and is supplied to the nonlinear reference state generator.

<u>Summary</u>. The seven reference states and their respective equations are listed below:

$$u_R = V \cos \alpha_R$$

$$w_R = V \sin \alpha_R$$

$$q_R = \dot{\alpha}_R + \dot{\gamma}_d$$

$$\Theta_R = \alpha_R + \gamma_d$$

$$\delta_R - \text{Eq (96)}$$

61

Δ_R - Eq (94)

h_d - reference path generator

Truth Model

In order to calculate the actual values of each of the seven states, a truth model is required. This section provides sets of equations which calculate the actual values for the seven state variables. Since the MOD6DF program (see Appendix D) integrates the specified equations, various first-order differential equations are developed.

Basic Equations. The force equation, Eq (92), is again used except it is solved in terms of $\dot{V}$ as

$$\dot{V} = \frac{T\cos\alpha - \bar{q}SC_D - mg\sin\gamma}{m} \tag{103}$$

This equation for $\dot{V}$ can be integrated to solve for actual velocity, V_A.

The normal force equation can be written (Ref 17:207)

$$mV\dot{\gamma} = L - mg\cos\gamma + T\sin\alpha \tag{104}$$

which can be solved for $\dot{\gamma}$ as

$$\dot{\gamma} = \frac{\bar{q}SC_L - mg\cos\gamma + T\sin\alpha}{mV} \tag{105}$$

Eq (105) may be integrated to yield the actual flight path angle, γ_A.

The moment equation can be used to solve for the pitch rate derivative. This equation, previously written in the form of Eq (88), may be rewritten as

$$\dot{q} = \frac{C_m \bar{q} S \bar{c}}{I_y}$$
(106)

Eq (106) may be integrated to compute the actual pitch rate, q_A. Then q_A can be used to find the actual pitch angle since

$$\dot{\Theta} = q$$
(107)

Referring back to Chapter V, Fig. 12 illustrates the relationship between $\dot{h}$, $\dot{R}$ and V. Previously derived equations for range and altitude derivatives are

$$\dot{R} = V \cos \gamma$$
(37)

and

$$\dot{h} = V \sin \gamma$$
(36)

Integration of Eqs (37) and (36) result in actual range, R_A, and actual altitude, h_A, respectively.

The actual elevator deflection, δ_A, is computed by integrating

$$\dot{\delta}_A = - \frac{\delta_A}{\tau_e} + \left(\frac{\delta_R}{\tau_e} + \frac{\delta \delta_c}{\tau_e} \right)$$
(108)

where τ_e is the time constant and δ_R is the reference elevator deflection.

Likewise, the actual thrust is found by integrating

$$\dot{\Delta}_A = -\frac{\Delta_A}{\tau_P} + \left(\frac{\Delta_R}{\tau_P} + \frac{\delta\Delta_c}{\tau_P}\right) \tag{109}$$

where τ_p is the time constant and Δ_R is the reference thrust.

Actual States. For convenience, the equations for each of the seven actual states are summarized below:

For velocity, U, the equation is

$$U_A = V_A \cos \alpha_A \tag{110}$$

where V_A is actual velocity and α_A is computed from

$$\alpha_A = \Theta_A - \gamma_A \tag{111}$$

Normal velocity, w, is

$$w_A = V_A \sin \alpha_A \tag{112}$$

For pitch rate, q, the equation is

$$q_A = \int \left(\frac{C_m \bar{\bar{q}} S \bar{c}}{I_y}\right) dt \tag{113}$$

For pitch angle, Θ, the equation is

$$\Theta_A = \int q_A \, dt \tag{114}$$

The actual elevator deflection is

$$\delta_A = \int \left[-\frac{\delta_A}{\tau_e} + \left(\frac{\delta_R}{\tau_e} + \frac{\delta \delta_c}{\tau_e} \right) \right] dt \tag{115}$$

The actual thrust is

$$\Delta_A = \int \left[-\frac{\Delta_A}{\tau_p} + \left(\frac{\Delta_R}{\tau_p} + \frac{\delta \Delta_c}{\tau_p} \right) \right] dt \tag{116}$$

And the actual altitude, h, is

$$h_A = \int \left(V_A \sin \gamma_A \right) dt \tag{117}$$

Initial Conditions. In order to integrate each of
the first order differential equations some initial
conditions must be set. These are designated below for
each of the quantities which is integrated:

$\gamma_o = 0$ rad $\qquad\qquad$ $\Theta_o = .066$ rad

$V_o = 647.3$ ft/sec $\qquad$ $\delta_{A_o} = -.065$ rad

$q_o = 0$ rad/sec $\qquad\quad$ $\Delta_{A_o} = 4729$ lbs

$h_o = 500$ ft $\qquad\qquad$ $R_o = 0$ ft

Computation of Updated Control

Now that the reference states and the actual states
have been computed it is appropriate to use both to find
the new control. With reference to Fig. 13 of this
chapter, the state deviation vector, $\delta \underline{x}$, can be computed

65

by differencing the reference and truth state vectors. The feedback gain matrix, G, has been computed from the linear model in Chapter III and can be multiplied by the state deviation vector, $\delta \underline{x}$, so that

$$\delta \underline{u} = G \delta \underline{x} \tag{118}$$

Eq (118) is the control law which calculates the feedback commands for the elevator and engine.

Both the total elevator control, δ, and the total thrust control, Δ, are computed by addition of the respective feedback command to the reference command

$$\delta = \delta_R + \delta\delta \tag{119}$$

and

$$\Delta = \Delta_R + \delta\Delta \tag{120}$$

This update of the two controls then completes one cycle of the nonlinear model computation leading to a new set of controls. The new control values are now used to adjust the reference states and the actual states as the simulation progresses in time along the range direction.

VII. Results

This chapter presents the results of the design study of the proposed optimal terrain following controller using a cubic spline reference path. The chapter is organized into three main sections. The first section shows the resultant numerical data for the system matrices. The second section illustrates the performance of the linearized model. And, in the third section an evaluation is made of the nonlinear controller model.

System Matrices

The open loop dynamics matrix, A, and the control distribution matrix, B, have been discussed previously. In this section the actual numerical values of each matrix are presented. The A matrix of Eq (27) is shown in Fig. 20. The B matrix of Eq (28) is illustrated in Fig. 19 below.

$$
B \;=\;
\begin{bmatrix}
0. & 0. \\
0. & 0. \\
0. & 0. \\
0. & 0. \\
10. & 0. \\
0. & 1. \\
0. & 0.
\end{bmatrix}
$$

Figure 19. The Control Distribution Matrix, B

$$
A = \begin{bmatrix}
-.007578 & .01276 & .034 & -32.178 & -.000314 & .000713 & 0. \\
-.1029 & -.8198 & 645.1 & 0. & -48.4 & -3.61E\text{-}05 & 0. \\
-.00013 & -.006086 & -.201 & 0. & -4.477 & 0. & 0. \\
0. & 0. & 1. & 0. & 0. & 0. & 0. \\
0. & 0. & 0. & 0. & -10. & 0. & 0. \\
0. & 0. & 0. & 0. & 0. & -1. & 0. \\
0. & -1. & 0. & 647.3 & 0. & 0. & 0.
\end{bmatrix}
$$

Figure 20. Open Loop Dynamics Matrix, A

68

The Output Matrix. In Chapter III the vector $\delta \underline{y}$ was shown to be the output deviation vector. The output deviation, $\delta \underline{y}$, for this thesis consists of the following four output variables:

(a) δh - altitude deviation

(b) $\delta \dot{h}$ - vertical velocity deviation

(c) $\delta \ddot{h}$ - vertical acceleration deviation

(d) δu - forward speed deviation

The two variables $\delta \dot{h}$ and $\delta \ddot{h}$ were sized by dividing these terms by V_o and V_o^2 respectively. The four output variable equations are shown below.

$$\delta h = \delta h \tag{121}$$

$$\frac{\delta \dot{h}}{V_o} = \frac{1}{V_o}\left(-\delta w + U \delta \theta\right) \tag{122}$$

$$\frac{\delta \ddot{h}}{V_o^2} = \frac{-1}{V_o^2}\left(Z_U \delta U + Z_w \delta w + Z_q \delta q + Z_\delta \delta \delta + Z_\Delta \delta \Delta\right) \tag{123}$$

$$\delta U = \delta U \tag{124}$$

These four output equations can be written in the form of Eq (6) in Chapter III as

$$\delta \underline{y} = \begin{bmatrix} 0. & 0. & 0. & 0. & 0. & 0. & 1. \\ 0. & \dfrac{-1}{V_0} & 0. & \dfrac{U}{V_0} & 0. & 0. & 0. \\ \dfrac{-Z_U}{V_0^2} & \dfrac{-Z_w}{V_0^2} & \dfrac{-Z_q}{V_0^2} & 0. & \dfrac{-Z_\delta}{V_0^2} & \dfrac{-Z_\Delta}{V_0^2} & 0. \\ 1. & 0. & 0. & 0. & 0. & 0. & 0. \end{bmatrix} \delta \underline{x} \tag{125}$$

When the numerical values are substituted the transformation matrix, C, used for this thesis is shown in Fig. 21.

Weighting Matrices Q and R. The method for determining the Q and R weighting matrices was discussed in Chapter III. Both matrices were developed in diagonal form. The final forms of the Q and R matrices are shown in Figs. 22 and 23. These values resulted from the iterations described in the next paragraph.

The Bryson and Ho method (Ref 4:149) was used to estimate reasonable values for the diagonal elements.

$$
C = \begin{bmatrix}
0. & 0. & 0. & 0. & 0. & 1.0 \\
0. & -.001539 & 0. & 1.0 & 0. & 0. \\
2.435\text{E}{-07} & 1.94\text{E}{-06} & 5.148\text{E}{-06} & 0. & 1.146\text{E}{-04} & 8.544\text{E}{-11} \\
1.0 & 0. & 0. & 0. & 0. & 0.
\end{bmatrix}
$$

Figure 21. Transformation Matrix, C

```
.25          0.          0.          0.

0.          1056.        0.          0.

0.          0.          2.78E09      0.

0.          0.          0.          6.25E-04
```

Figure 22. The Q weighting matrix

```
10.          0.

0.          2.5E-07
```

Figure 23. The R weighting matrix

Then these values were perturbed in attempting to achieve good performance for the controller. The corresponding maximum allowable deviations associated with the Q and R diagonal elements are shown in Figs. 24 and 25.

State Deviation Weighting Matrix. In Chapter III the cost function was written in terms of $\delta\underline{x}$ and $\delta\underline{u}$. This required the state deviation weighting matrix, P, which was shown to be equivalent to $C^T QC$. This matrix with its numerical values is shown in Fig. 26.

Computations of OPTSYS. Using all the system matrices and the weighting matrices, the OPTSYS program calculated the optimal steady-state gains for the terrain following controller and computed the eigenvalues of the system.

The steady-state Ricatti gain matrix, S, is presented in Fig. 27 and the feedback gain matrix, G, is shown in Fig. 28.

The seven eigenvalues of the open loop dynamics matrix, A, are shown in Fig. 29. All the open loop eigenvalues are stable.

The closed loop dynamics matrix, A+BG, results in eigenvalues which have been moved further into the stable region of the complex plane. This increase in stability is shown by comparison with the corresponding open loop eigenvalues in Fig. 29. The dominant complex roots produce a damping factor close to .707. This damping factor was desired so that the system would possess good time response and damping with minimal peak overshoot. It was

73

Diagonal Element	Maximum Deviation
q_{11}	$\delta h = 2 \text{ ft}$
q_{22}	$\dfrac{\delta \dot{h}}{V_o} = \dfrac{20 \text{ ft/sec}}{650 \text{ ft/sec}}$
q_{33}	$\dfrac{\delta \ddot{h}}{V_o^2} = \dfrac{8 \text{ ft/sec}^2}{(650 \text{ ft/sec})^2}$
q_{44}	$\delta U = 40 \text{ ft/sec}$

Figure 24. Q Matrix Maximum Deviations

Diagonal Element	Maximum Deviation
r_{11}	$= .316 \text{ rad}$
r_{22}	$= 2000 \text{ lbs}$

Figure 25. R Matrix Maximum Deviations

7.899E-04	.001314	.003486	0.	.07756	5.78E-03	0.
.001314	.01297	.02777	-1.625	.6179	4.609E-07	0.
.003486	.02777	.07367	0.	1.639	1.223E-06	0.
0.	-1.625	0.	1056.	0.	0.	0.
.07756	.6179	1.639	0.	36.48	2.721E-05	0.
5.795E-03	4.609E-07	1.223E-06	0.	2.721E-05	2.03E-11	0.
0.	0.	0.	0.	0.	0.	.25

Figure 26. State Deviation Weighting Matrix, $C^T Q C$

75

.01593	-.002726	.0996	2.289	-.00721	1.166E-05	.00389
-.00273	.078	-1.572	-59.73	.1167	-1.418E-06	-.115
.09951	-1.572	80.63	1451.	-9.178	4.531E-05	2.464
2.289	-59.73	1451.	47172.	-108.3	.00114	89.87
-.00721	.1167	-9.178	-108.3	2.426	-3.302E-06	-.1581
1.166E-05	-1.418E-06	4.531E-05	.001142	-3.3E-06	8.189E-09	1.898E-06
.003889	-.116	2.464	89.87	-.1581	1.89E-05	.2647

Figure 27. Steady-state Ricatti gain matrix, S

$$\begin{bmatrix} .0072 & -.1167 & 9.176 & 108.3 & -2.426 & 3.302E-06 & .1581 \\ -46.64 & 5.675 & -181.3 & -4567.8 & 13.21 & -.03275 & -7.593 \end{bmatrix}$$

Figure 28. The Feedback Gain Matrix, G

Open Loop	Closed Loop
$-.51127 + 1.9556j$	$-6.498 + 1.47j$
$-.51127 - 1.9556j$	$-6.498 - 1.47j$
$-.00292 + .0635j$	$-1.431 + 1.399j$
$-.00292 - .0635j$	$-1.431 - 1.399j$
$-10.$	-19.426
$0.$	$-.0358$
$-1.$	$-.999$

Figure 29. Eigenvalues of the System

also required that the system not be overly damped since that would cause excessive acceleration and undue crew discomfort.

Stability of the Linearized Perturbation Equations

A computer program was developed to verify the stability of the linearized perturbation equations derived in Chapter IV. Since the coefficients in these equations determine the value of the A matrix and ultimately dictate the optimal feedback gains, it was important to insure their stability. The matrices A, B, G, and A+BG were used to simulate the system in closed loop form.

Since the linearized equations are in perturbation form a straight and level flight profile was assumed as the zero reference condition. Initial conditions were set on one of the seven perturbation state variables while the remaining six were set to zero. Then the seven differential equations (see Eqs (19) through (25)) were integrated from 0 to 20 seconds. In addition, Eq (122) was integrated to check the output vertical velocity performance. Figures 30, 31, 32, and 33 illustrate the linearized equations performance for an initial perturbation in x-direction velocity of 25 ft/sec. Figures 34 to 37 correspond to an initial perturbation in altitude of 25 feet. And, Figures 38 to 41 show how a perturbation of 200 lbs of thrust affects the closed loop linear model.

Also included in Figs. 42 to 45 are plots of the
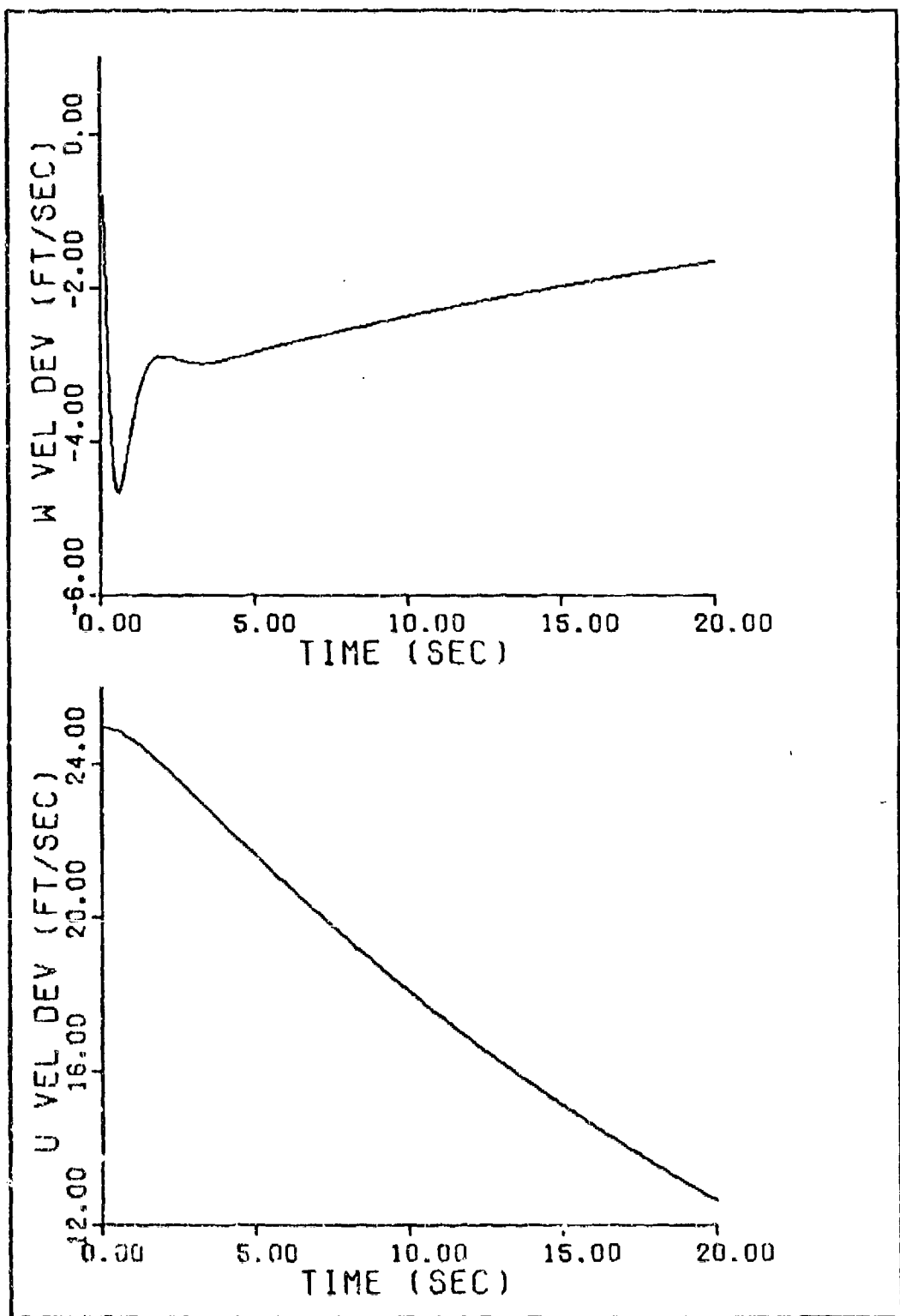
Figure 30. Response to x-direction Velocity Perturbation
of 25 ft/sec
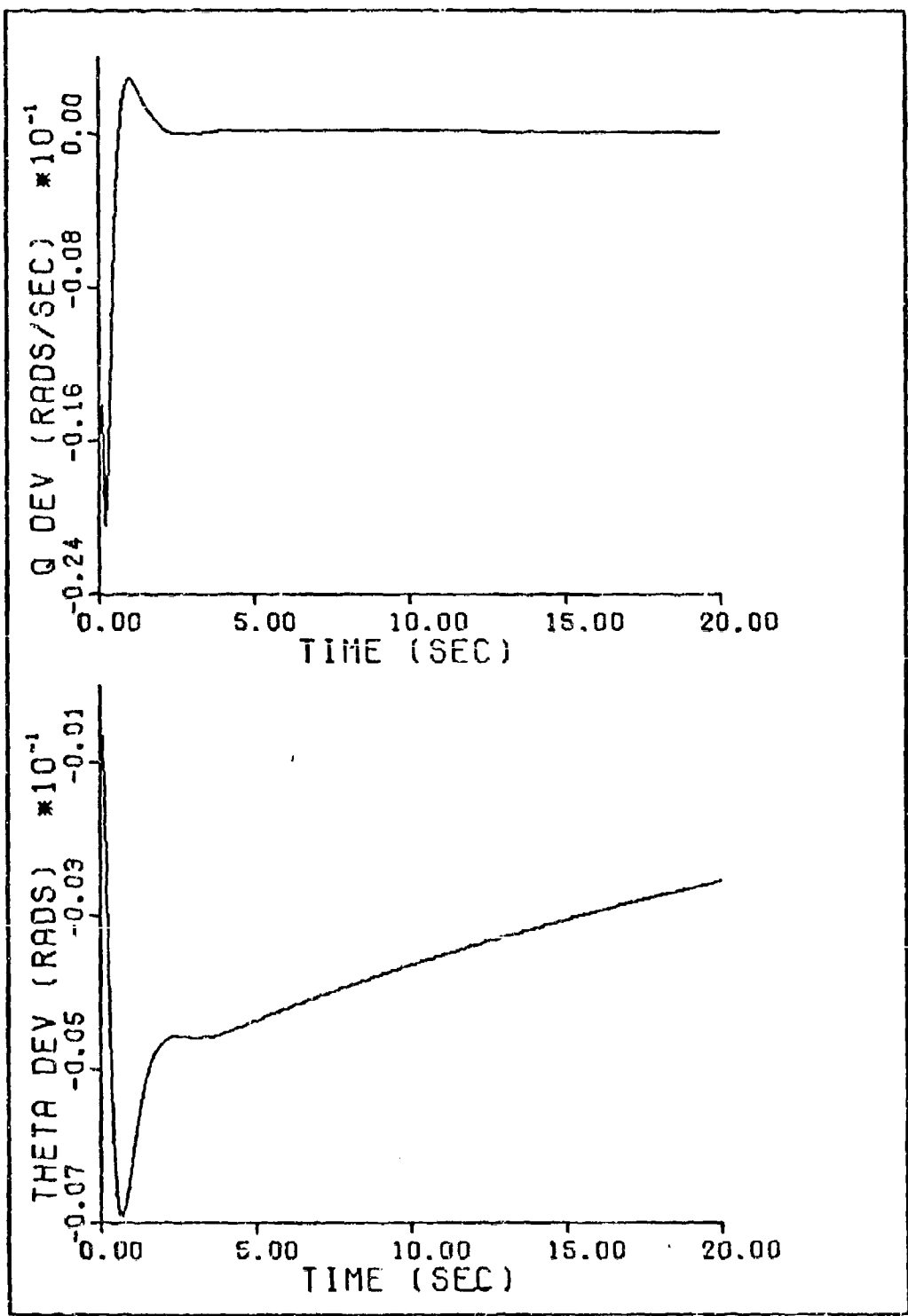
Figure 31. Response to x-direction Velocity Perturbation of 25 ft/sec

81
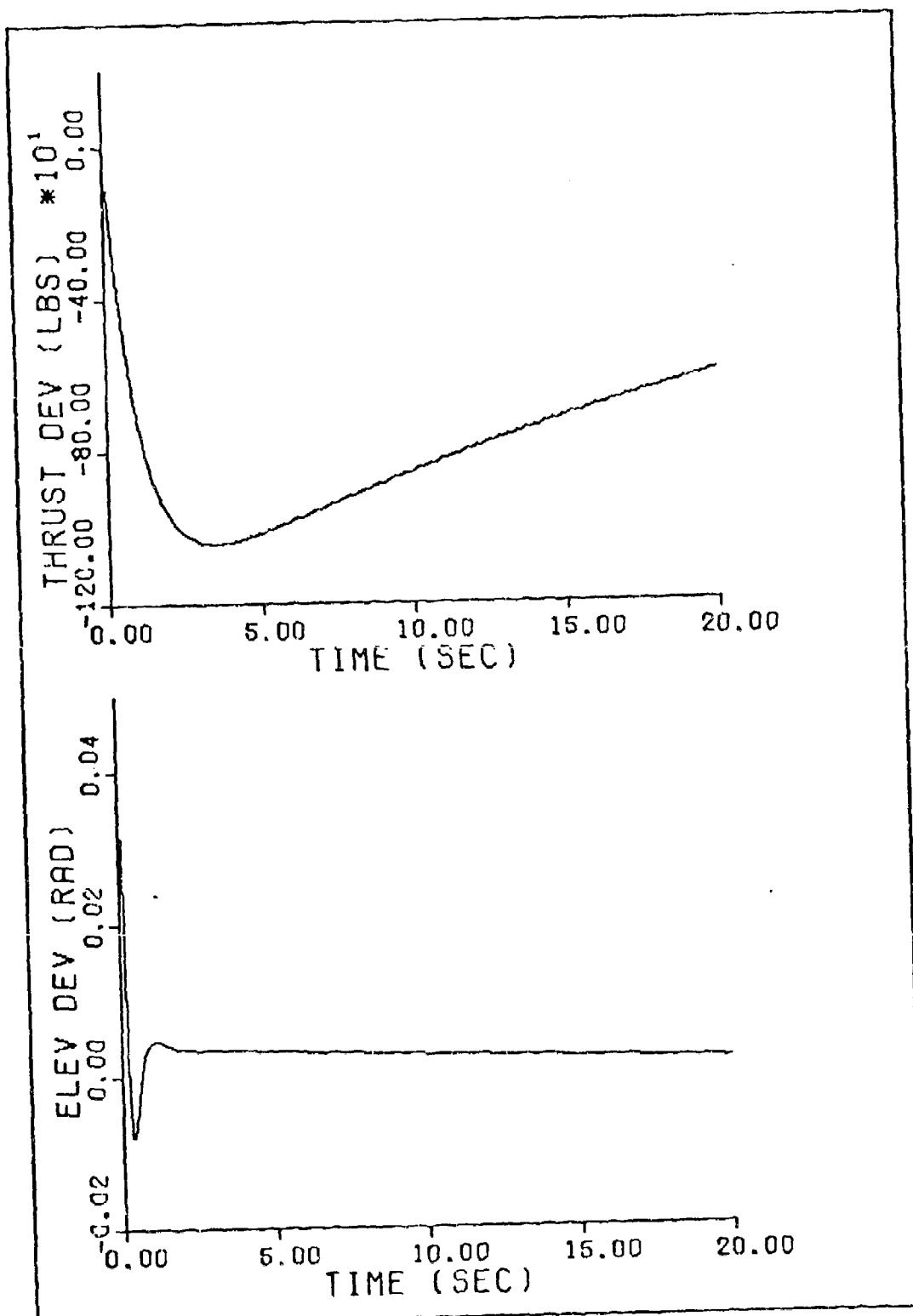
Figure 32. Response to x-direction Velocity Perturbation
of 25 ft/sec
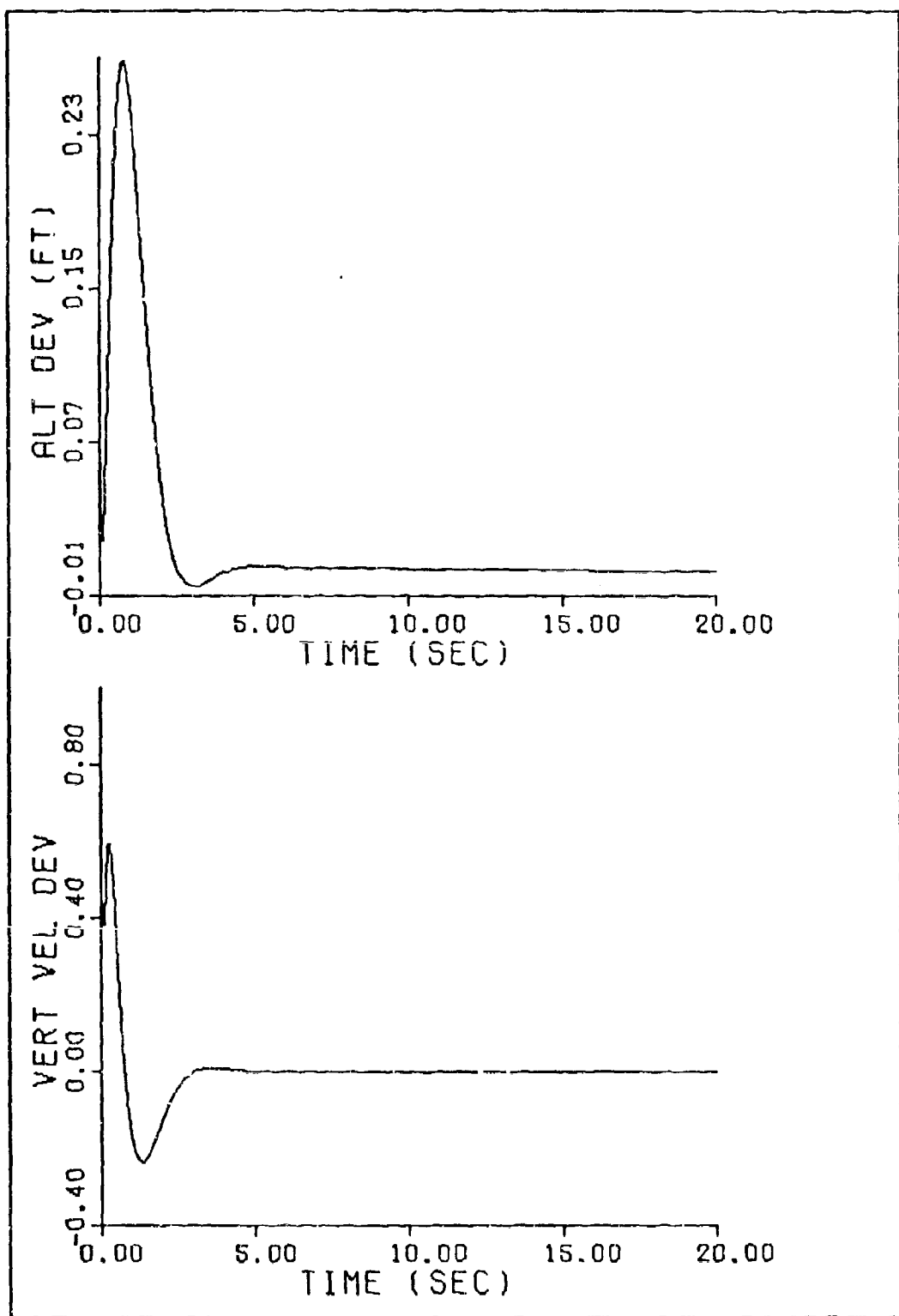
Figure 33. Response to x-direction Velocity Perturbation
of 25 ft/sec
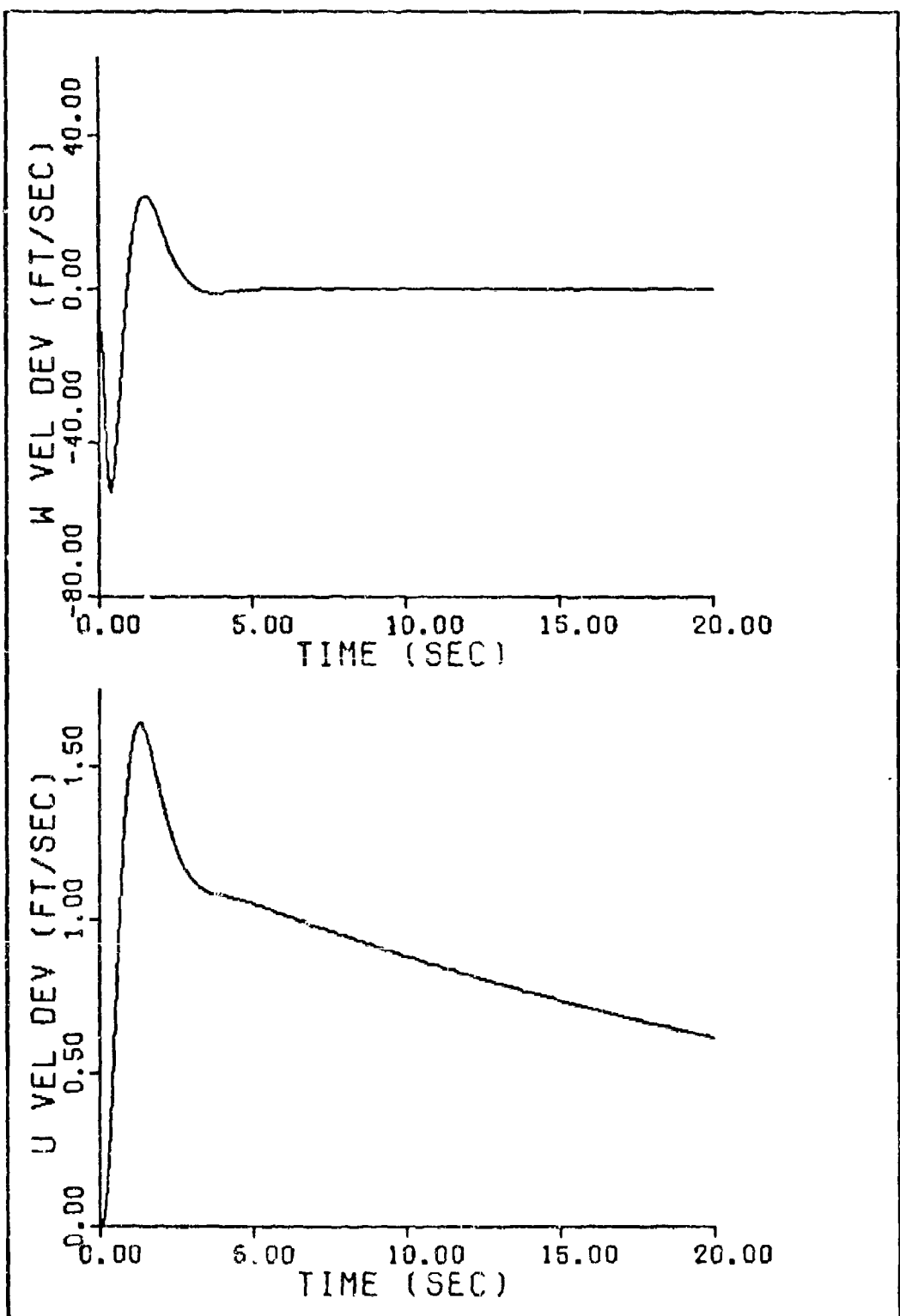
Figure 34. Response to Altitude Perturbation of 25 ft
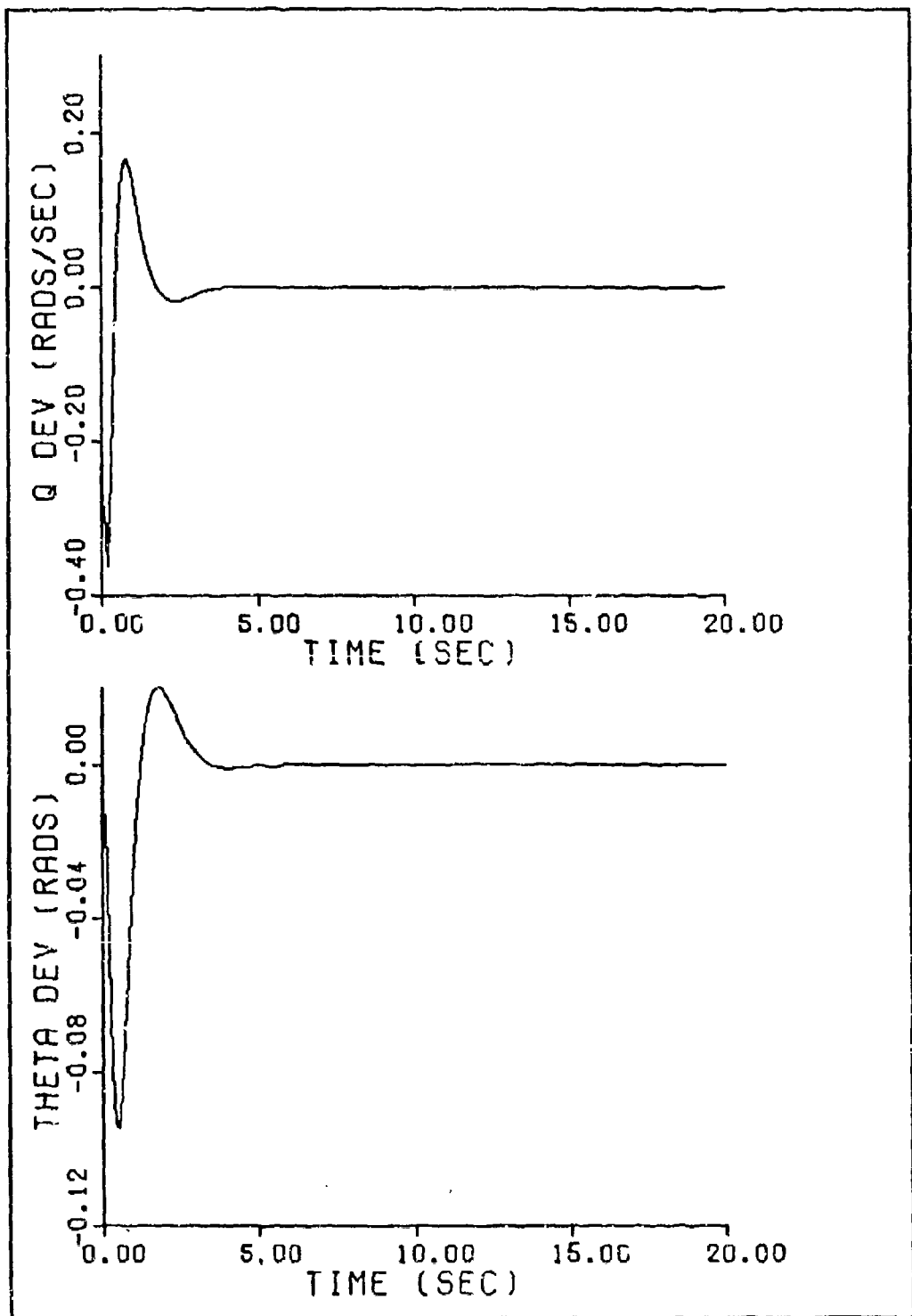
Figure 35. Response to Altitude Perturbation of 25 ft
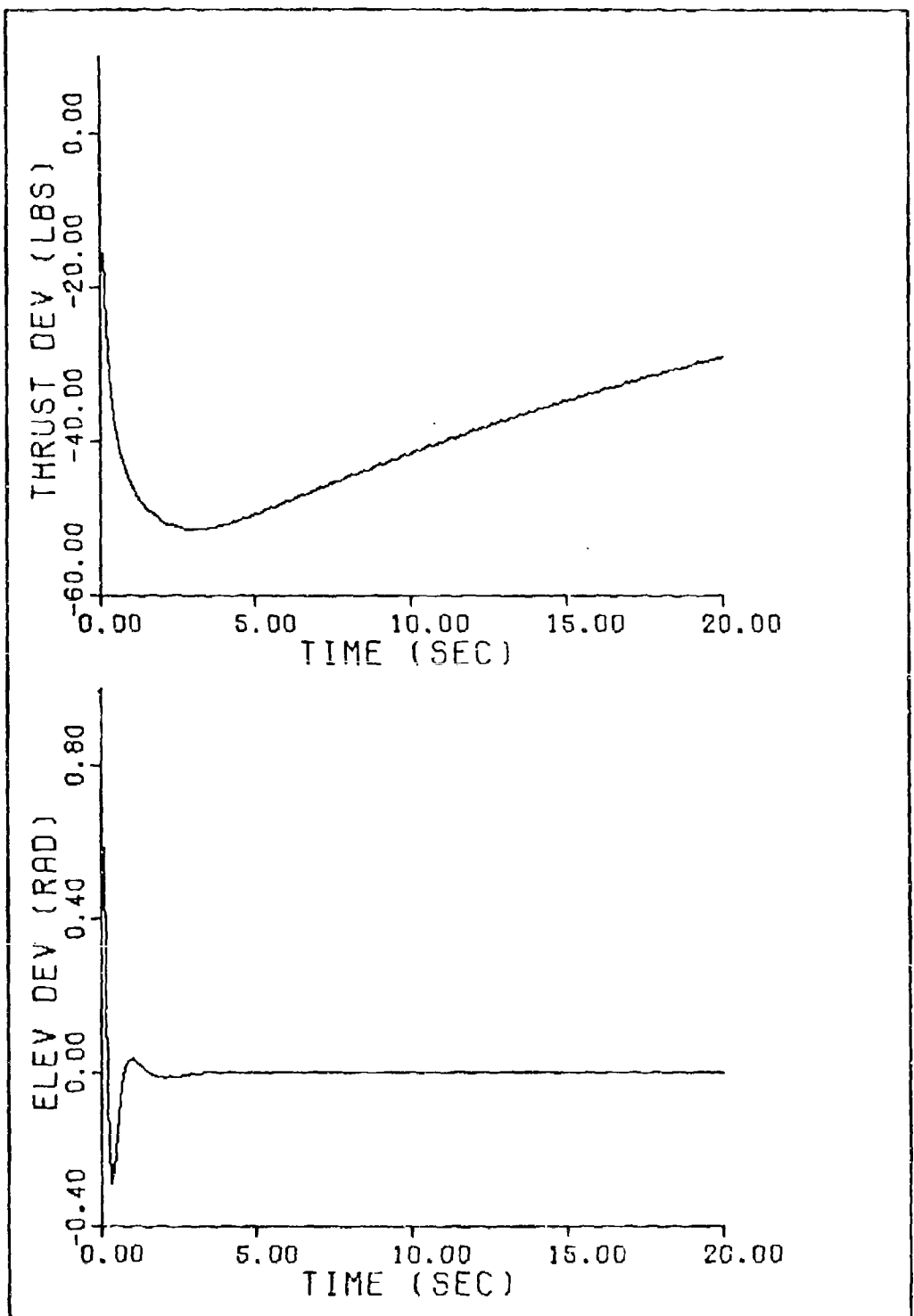
Figure 36. Response to Altitude Perturbation of 25 ft
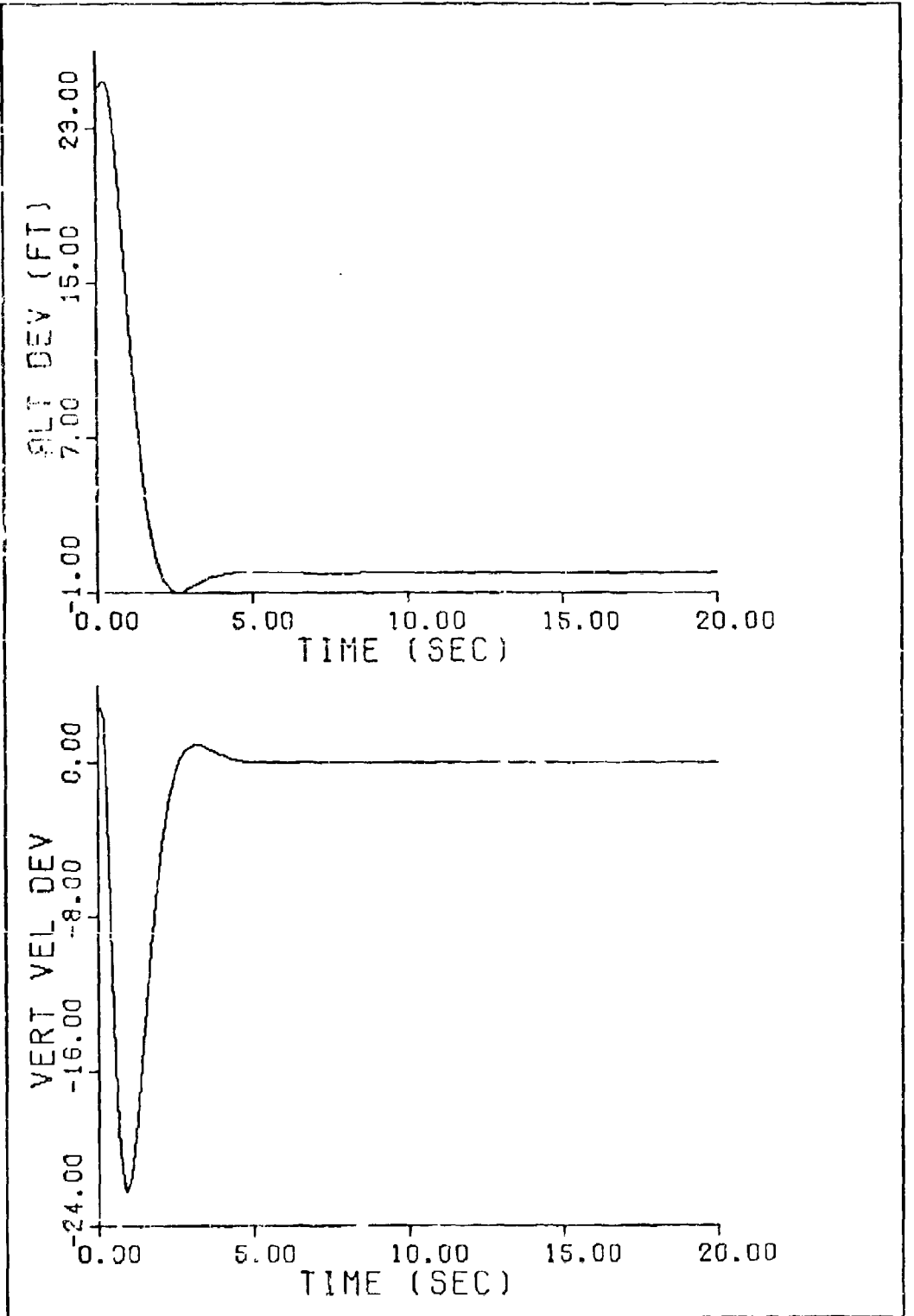
E ..e 37. Res .e ' Altitude Perturbation of 25 ft
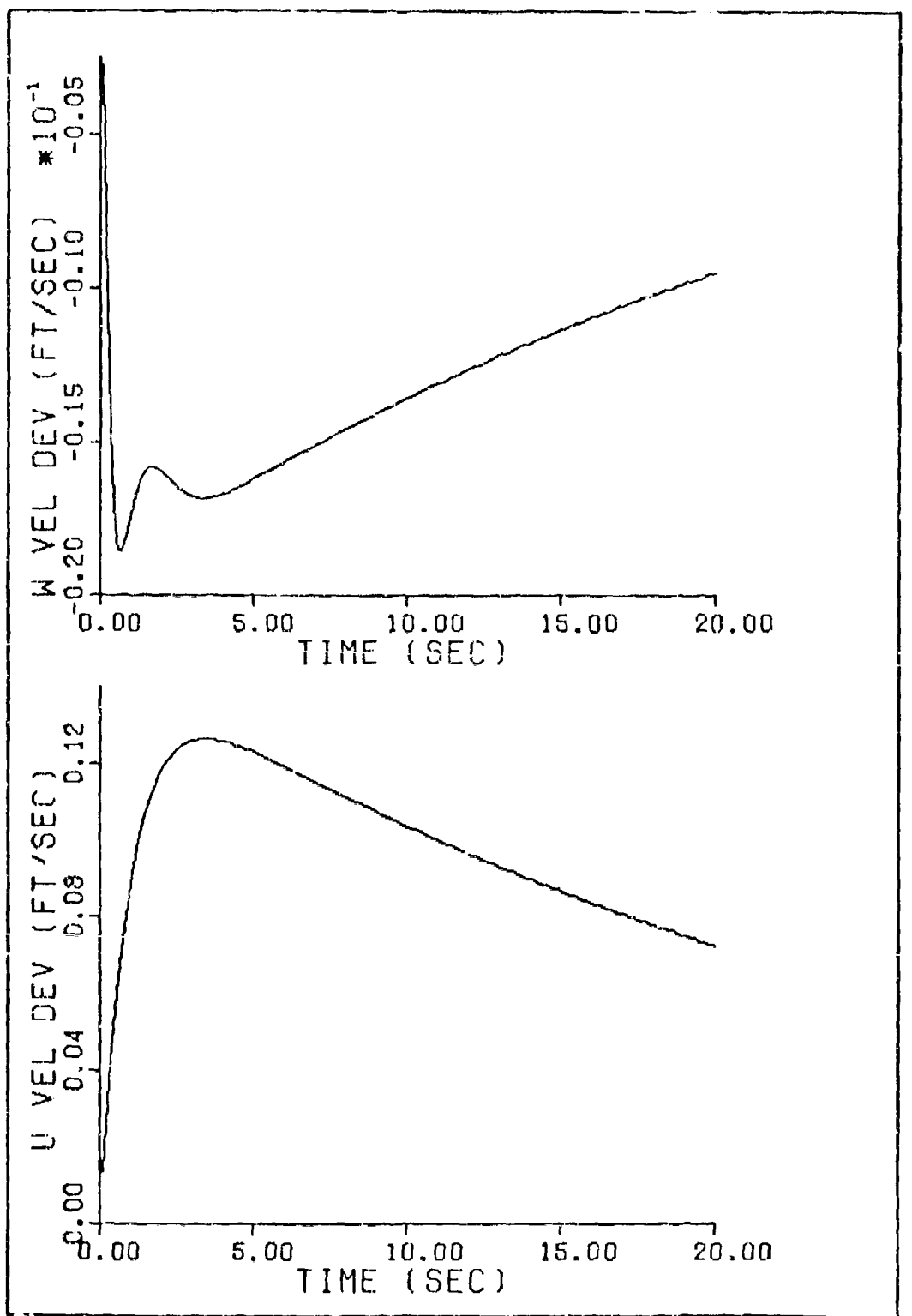
Figure 38. Response to Thrust Perturbation of 200 lbs

88
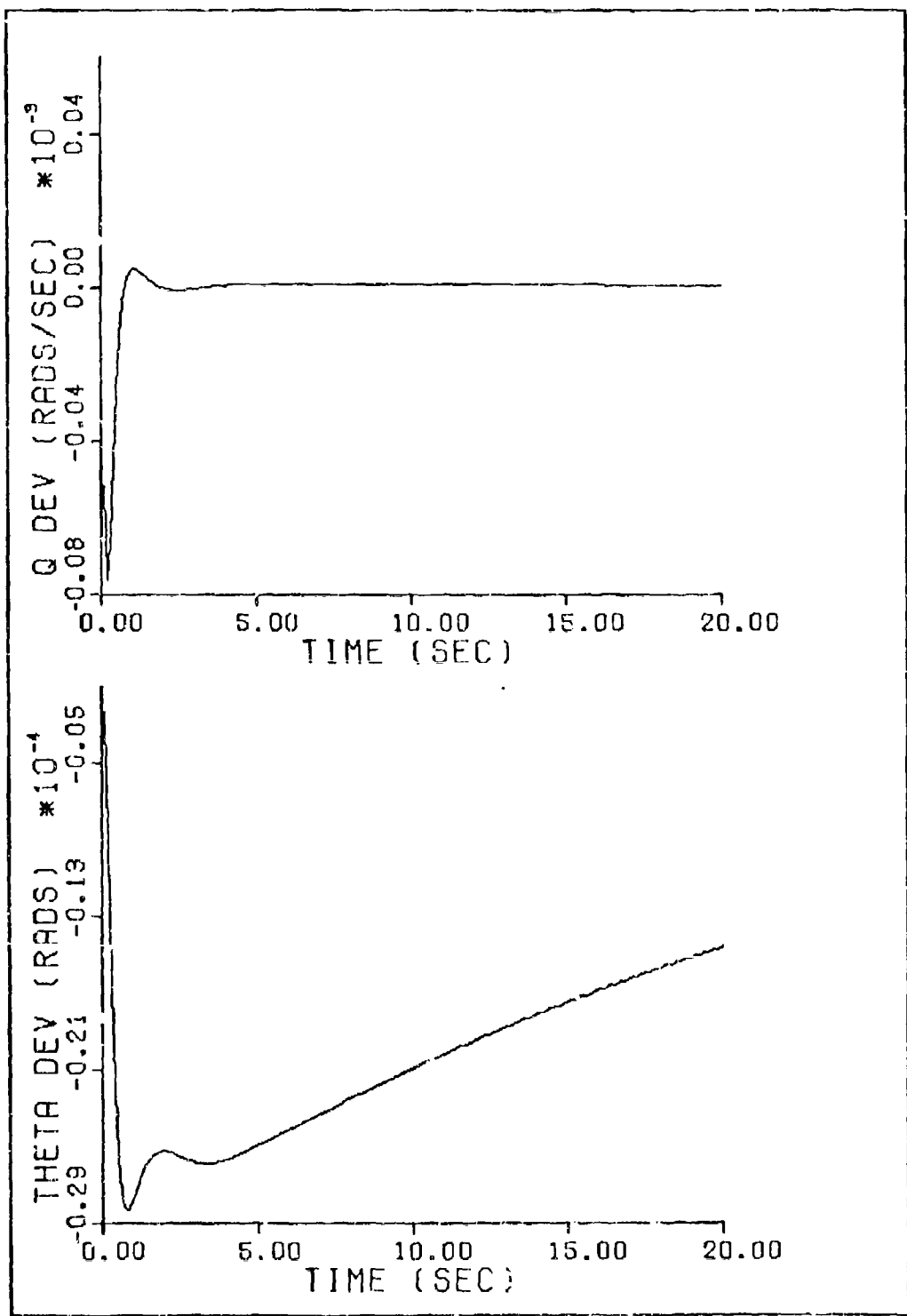
Figure 39. Response to Thrust Perturbation of 200 lbs
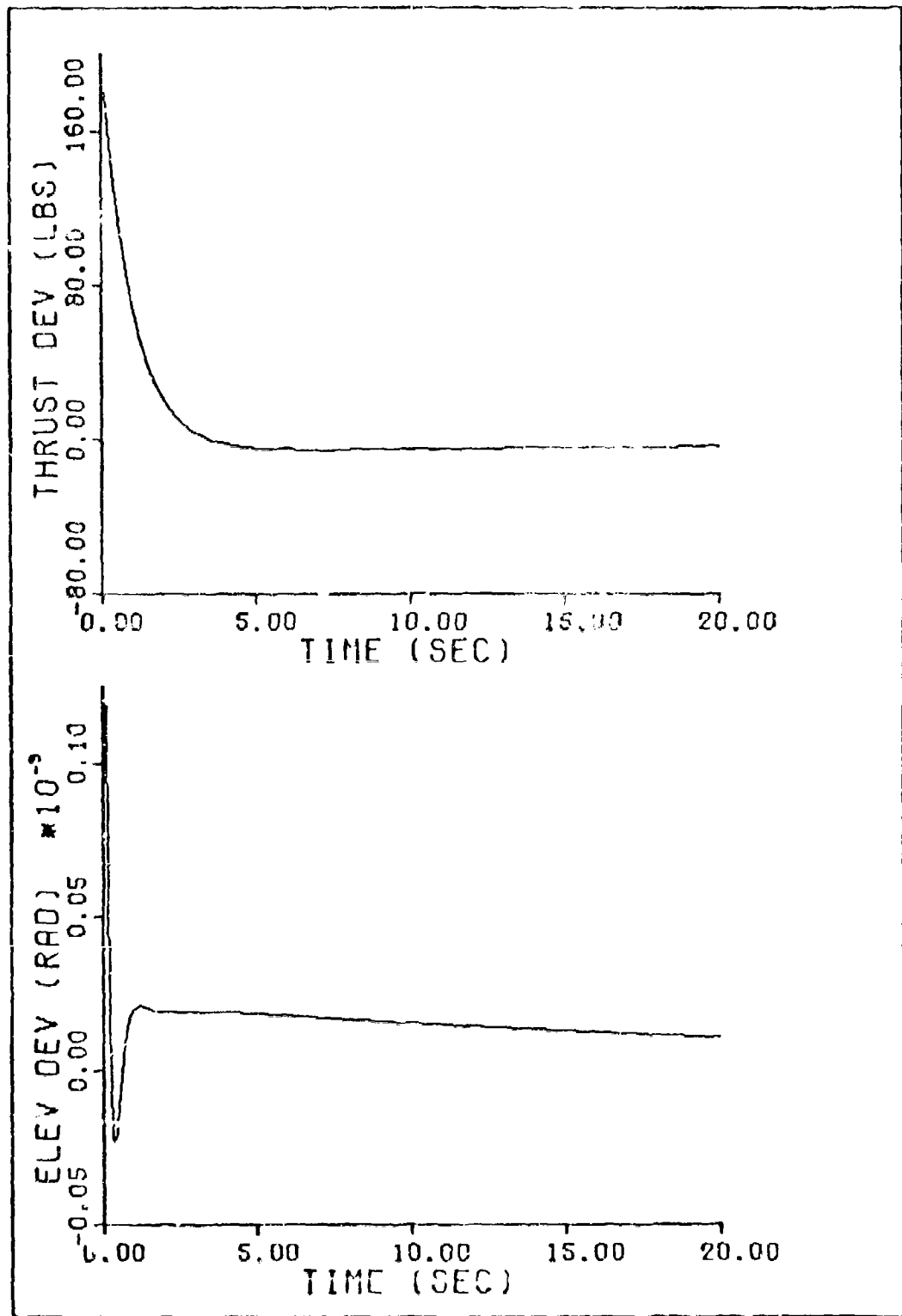
Figure 40. Response to Thrust Perturbation of 200 lbs

90
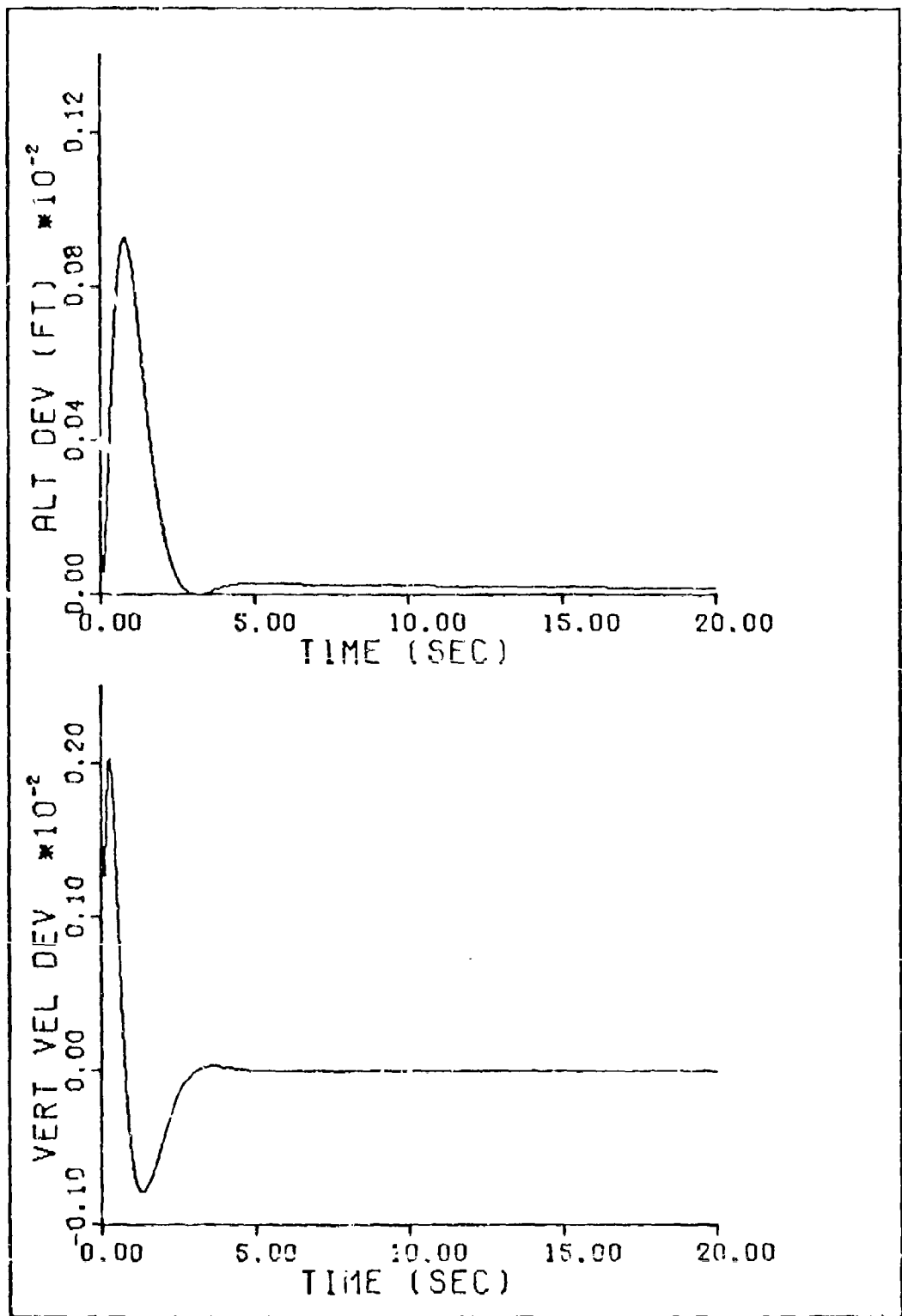
Figure 41. Response to Thrust Perturbation of 200 lbs
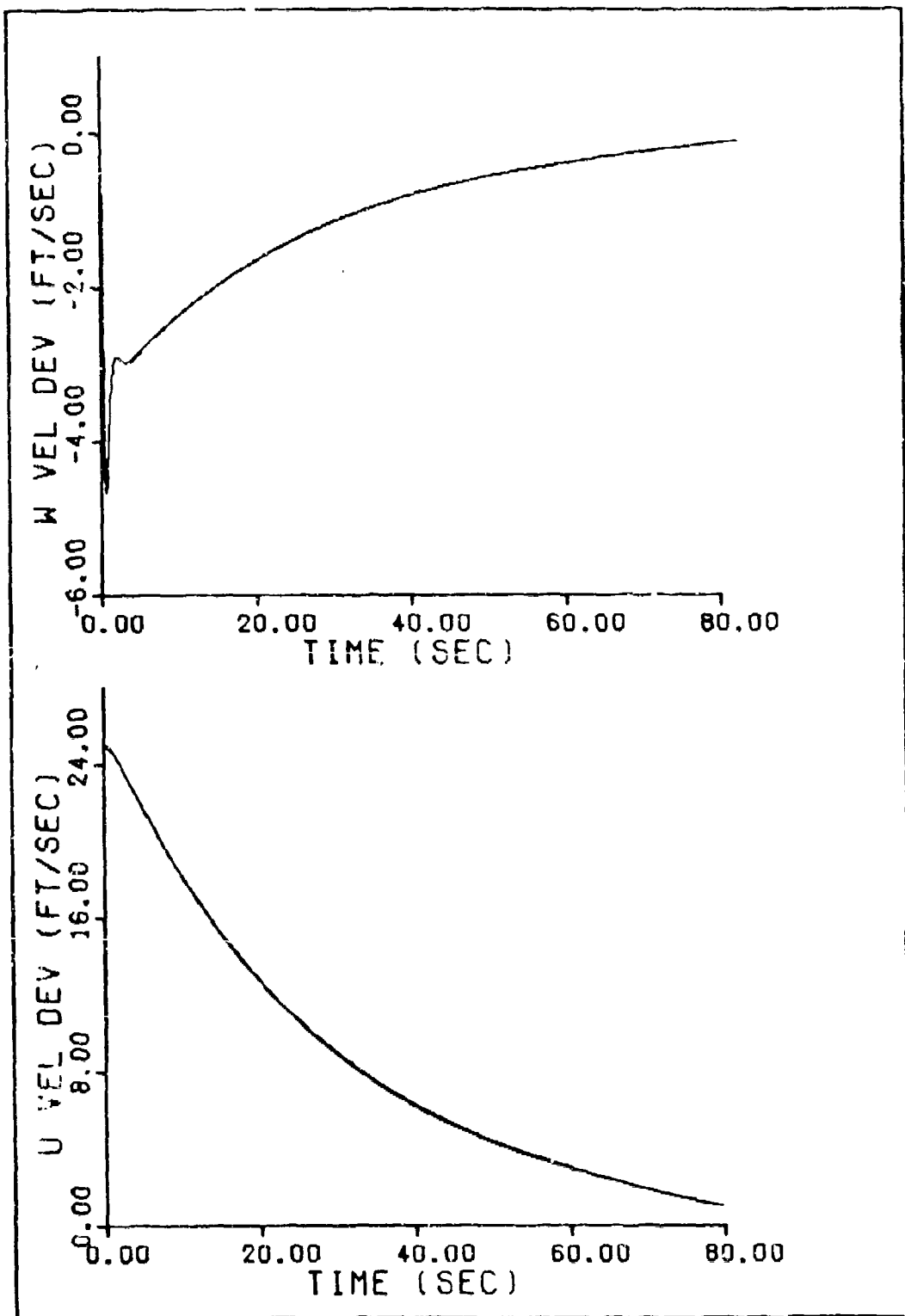
Figure 42. Steady-state Response to Velocity Perturbation
of 25 ft/sec
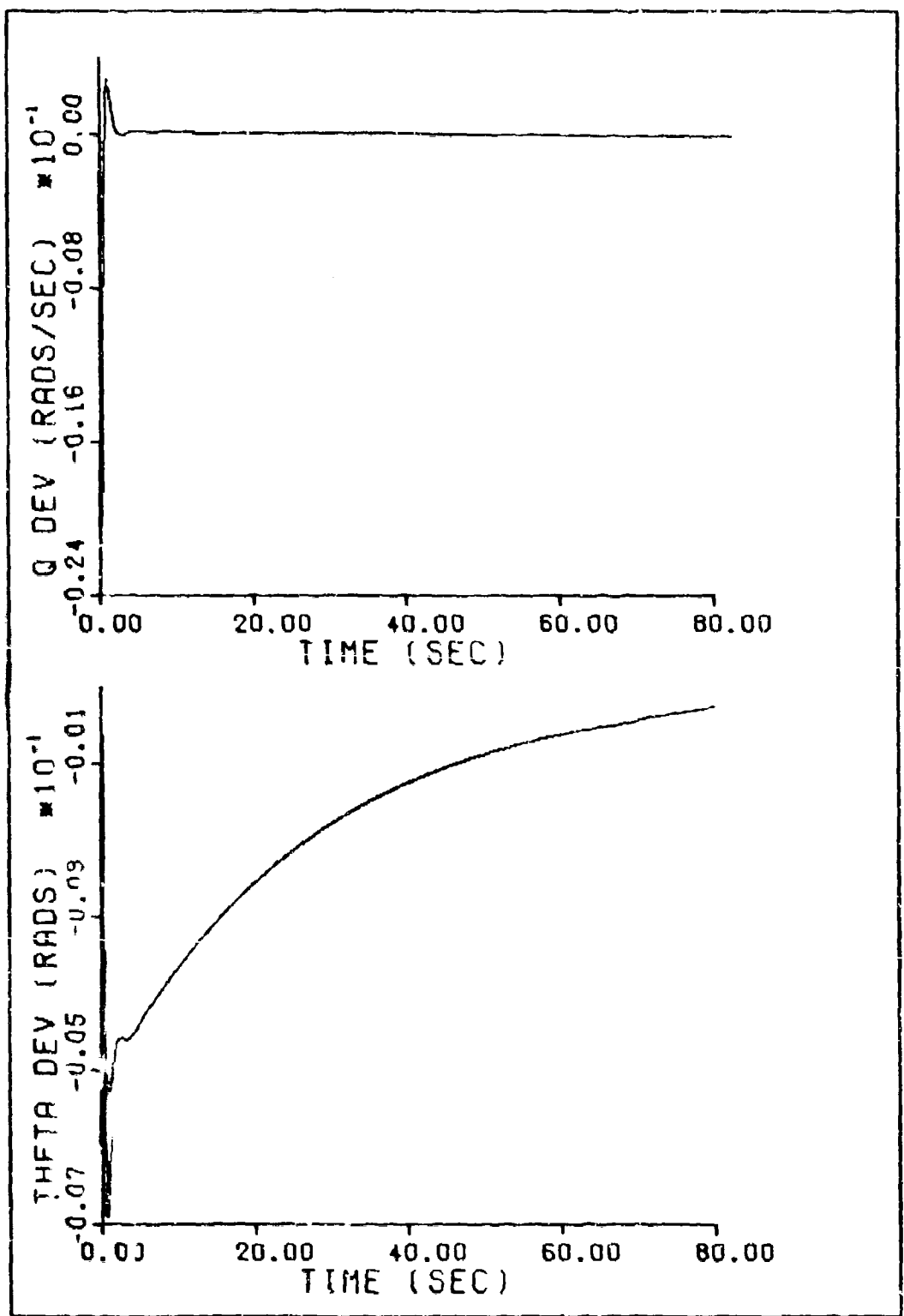
Figure 43. Steady-state Response to Velocity Perturbation
of 25 ft/sec

93
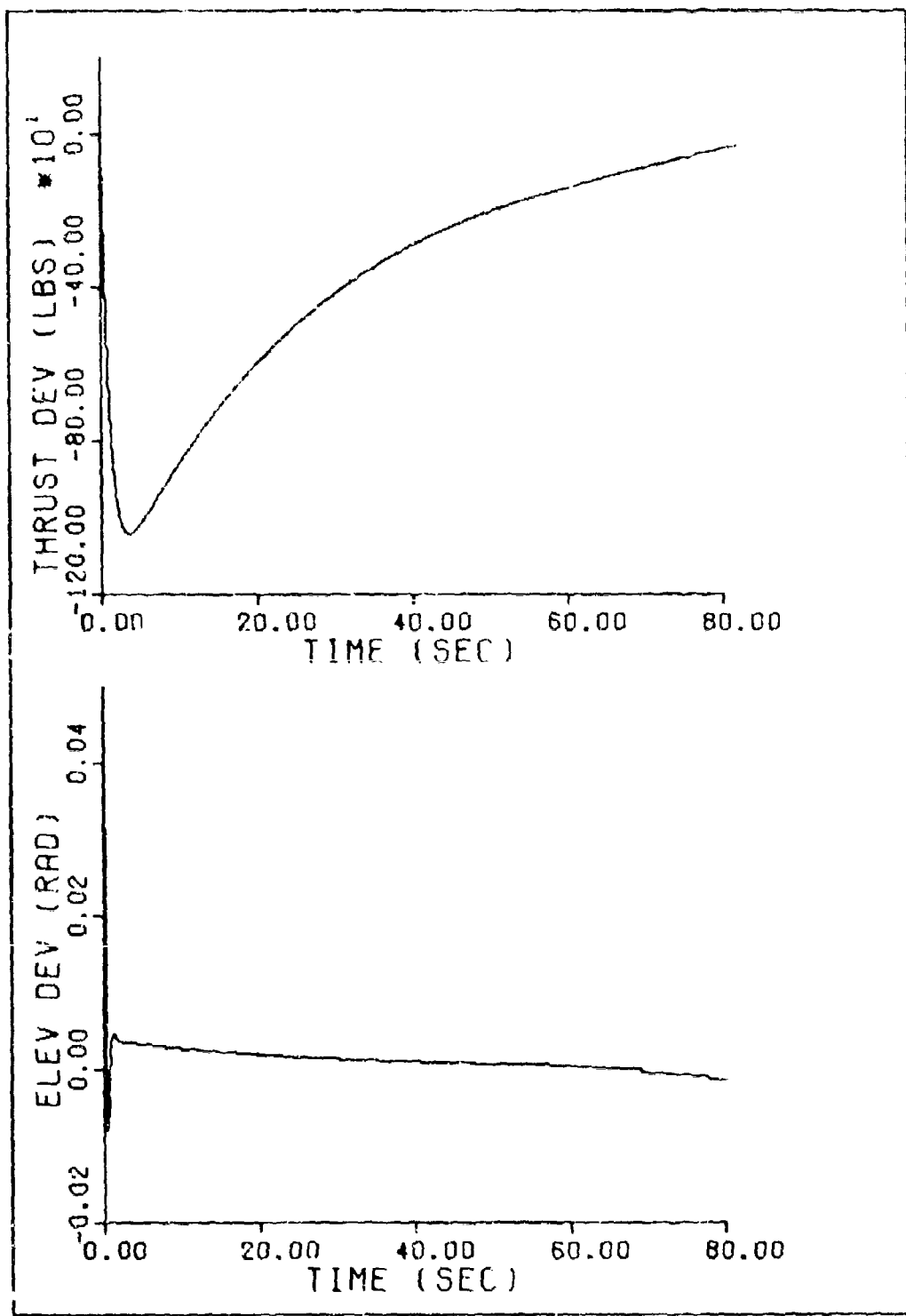
Figure 44. Steady-state Response to Velocity Perturbation
of 25 ft/sec

94
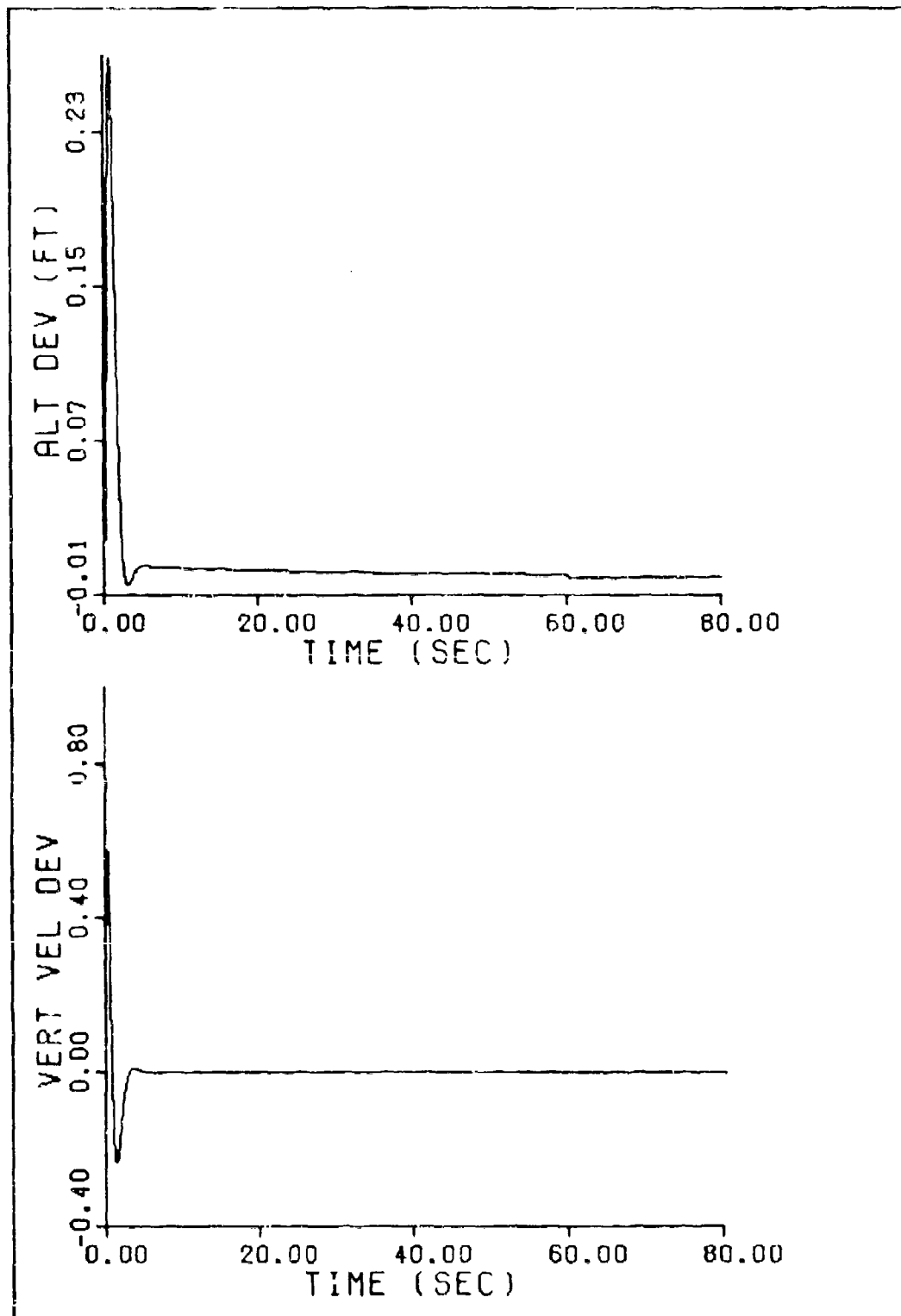
Figure 45. Steady-state Response to Velocity Perturbation
of 25 ft/sec

95

steady-state performance of the controller responding to an initial perturbation of 25 ft/sec in x-direction velocity. These plots show that in steady-state the controller restores all states to the zero flight conditions.

In all cases, the time response of the linear system is shown to be quite good. There are no large fluctuations in response and the system is restored to the zero reference in a reasonable amount of time.

Performance of the Nonlinear Controller

Much of the initial study of this thesis consisted of verification of the equations used in the nonlinear reference and truth models. Once these equations and the associated computer programs were investigated it was possible to evaluate the performance of the controller with the nonlinear reference and truth models.

The MOD6DF program was used to compute a simulated reference path for the controller. This simulated path consisted of a simple pullup maneuver in which an aircraft climbs over an obstacle and levels off. This is shown in Fig. 46. For this simple pullup maneuver the acceleration and g rate limits can be varied and the duration of the pullup can be specified.

Two different reference generation schemes were developed. One involved a cubic spline path and the other was a quartic (polynomial of degree four) spline
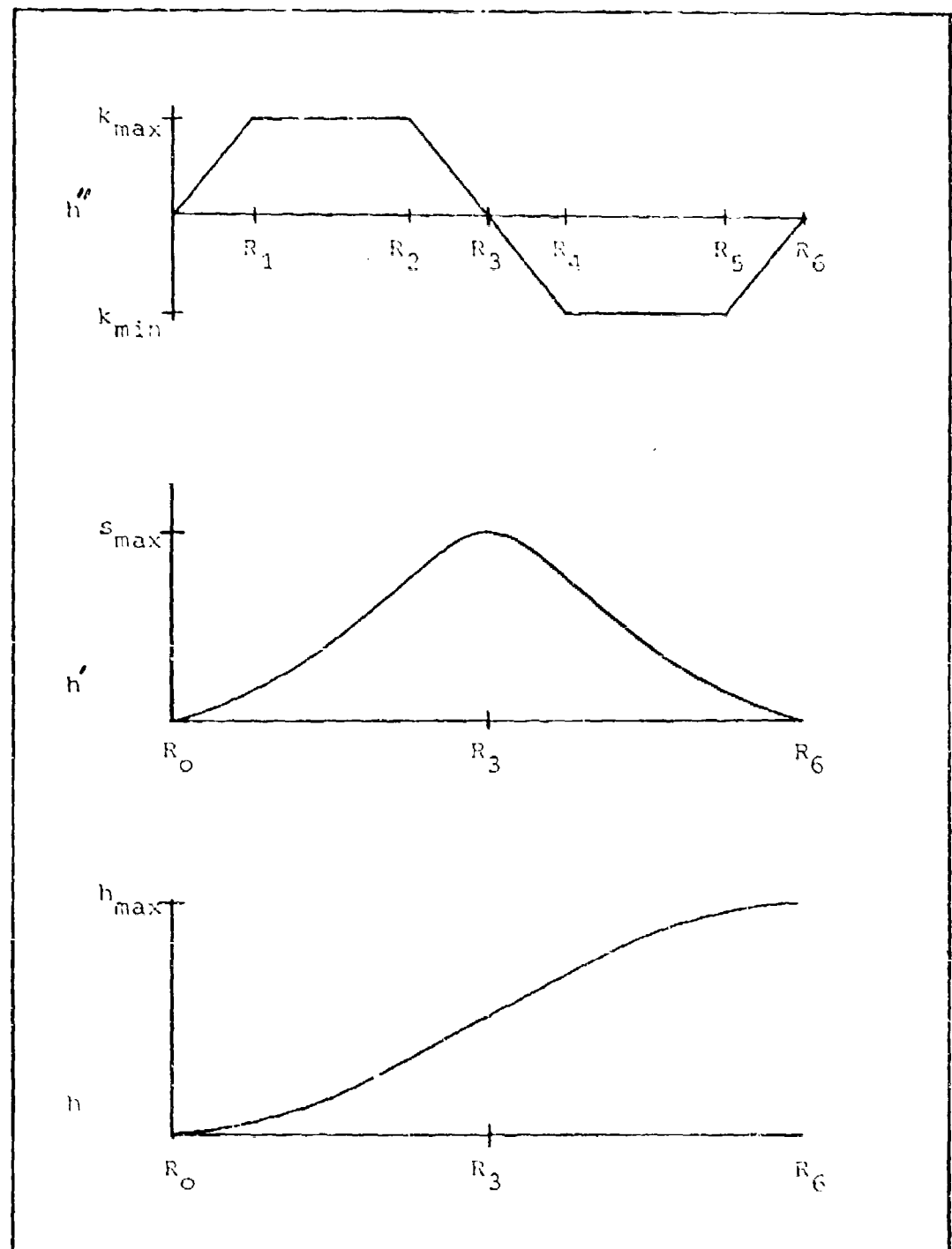
Figure 46. Generation of Simple Pullup Maneuver

path. Modules were designed for program MOD6DF which
consisted of a spline path generation routine and a
corresponding interpolation routine. These reference
path generation subroutines were then linked to the
nonlinear controller model to evaluate performance.

For the quartic spline reference pullup maneuver the
initial altitude was 500 feet. Over a range of 10,000
feet the aircraft climbed 1090 feet to level off. The
specified limits on k (see Fig. 46) were .5g for this
profile. The resulting quartic reference path was tracked
by the controller with a maximum altitude error of 6 feet.
The velocity deviation was less than 2 ft/sec at level
off. Both the altitude and velocity tracking errors were
regulated to zero after completion of the pullup maneuver.
The velocity error settling time was slightly longer than
the altitude settling time after level off.

The cubic spline pullup maneuver was also performed
for a .5g limit on k. Over a range of 9,000 feet the
cubic spline reference path increased in altitude from
500 feet to 1280 feet. The optimal controller tracked
the reference altitude within 4.5 feet. The velocity
tracking error for the cubic spline reference pullup was
less than 2 ft/sec. Like the quartic pullup maneuver,
both the velocity error and the altitude error were nulled
after level off by the feedback controller.

The optimal controller was next flown using the
optimized cubic spline reference path described in

98

Chapter V. Over the first 15,000 feet of this terrain profile the standard deviation in altitude was 160 feet. The optimal controller was capable of maintaining the altitude tracking error at less than 1.5 feet and kept the velocity tracking error less than 1.5 ft/sec. This was very good performance even though the terrain was rather benign. The thrust fluctuation was reduced when compared to the Boeing optimal controller flying over a similar low level terrain profile. But the actual thrust did lag the required reference thrust because of the simplified thrust control system developed for this thesis.

In all the flight profiles flown by the optimal terrain following controller so far, the tracking errors have not been large and can be considered quite acceptable. Whenever an altitude tracking error exists the actual aircraft altitude has always been greater than the reference altitude thus promoting a safe terrain following mission. Even though these test profiles have not been long in duration they do show the potential for good controller performance using an optimized cubic spline reference path.

VIII. Conclusions and Recommendations

The feedback controller is a stable controller capable of tracking a cubic spline reference path. The cubic spline generator produces a reference path possessing good tracking quality. The resulting controller provides good path control and only slight tracking errors in altitude and velocity provided the state deviations remain in the linearized region about the nominal reference trajectory. By allowing variations in velocity, the thrust fluctuation is reduced. This is essential to increasing engine life and decreasing fuel consumption.

The weighting matrices, Q and R, are very influential in the performance of the terrain following controller. These matrices can be judiciously adjusted to strengthen the controller operation and cause the aircraft to fly closer to the reference path.

The following recommendations result from work on this design study

(a) investigate, through more sophisticated techniques like root square locus, the eigenvalue placement due to varying the Q and R matrices

(b) evaluate this nonlinear controller over a greater variety of terrain profiles

(c) investigate the linearizing assumptions made in Chapter IV and determine whether a rotating coordinate reference frame tangent to the

reference trajectory is more accurate

(d) develop a more sophisticated thrust and velocity
control system for improving the controller
performance

(e) modify the constant energy assumption to allow
variations in energy within a specified energy
envelope

Bibliography

1. Ahlberg, J. H., E. N. Nilson and J. L. Walsh. The Theory of Splines and Their Applications. New York: Academic Press, 1967

2. Ball, S. A., Jr. F-111 Operation in Terrain Following Mode. Eleventh Symposium Guidance and Control Panel, AGARD, NATO, Brussels, Belgium, 2 September 1970.

3. Bryson, A. E., Jr. and W. E. Hall Jr. Optimal Control and Filter Synthesis by Eigenvector Decomposition. Stanford University, California: Guidance and Control Laboratory, November 1971.

4. Bryson, A. E., Jr. and Yu-Chi Ho. Applied Optimal Control. Washington, D. C.: Hemisphere Publishing Corporation, 1975.

5. Diesel, J. W. and J. L. Griffin. Modularized Six-Degree-of-Freedom Computer Program, Version II. Woodland Hills, California: Litton Systems, Inc., March 1971.

6. Etkin, B. Dynamics of Atmospheric Flight. New York: John Wiley and Sons, Inc., 1972

7. ------. Dynamics of Flight. New York: John Wiley and Sons, Inc., 1959.

8. Fosth, D. C., M. S. Gerson and P. G. Williams. Optimal Integrated Terrain Following Study Technical Analysis. Seattle, Washington: Boeing Aerospace Company, November 1976.

9. Funk, J. E. Terrain Following Control Based on an Optimized Spline Model of Aircraft Motion. Wright-Patterson Air Force Base, Ohio: Aeronautical Systems Division, November 1975.

10. Kirk, D. E. Optimal Control Theory: An Introduction. Englewood Cliffs, New Jersey: Prentice-Hall, Inc., 1970.

11. Kisslinger, R. L. and G. J. Vetsch. "Manual Terrain-Following System Development for a Supersonic Fighter Aircraft." Journal of Aircraft, 3: 305-309 (July-August 1966).

12. Kolk, W. R. Modern Flight Dynamics. Englewood Cliffs, New Jersey: Prentice-Hall, Inc., 1961.

13. K akernaak, H. and R. Sivan. _Linear Optimal Control Systems_. New York: John Wiley and Sons, Inc., 1972.

14. McRuer, D., I. Ashkenas and D. Graham. _Aircraft Dynamics and Automatic Control_. Princeton, New Jersey: Princeton University Press, 1973.

15. Miele, A. _Flight Mechanics Volume I_. Reading, Massachusetts: Addison-Wesley Publishing Company, Inc., 1962.

16. Roskam, J. _Flight Dynamics of Rigid and Elastic Airplanes_. Lawrence, Kansas: Roskam Aviation and Engineering Corporation, 1972.

17. Seckel, E. _Stability and Control of Airplanes and Helicopters_. New York: Academic Press, Inc., 1964.

18. Shampine, L. F. and R. C. Allen. _Numerical Computing: An Introduction_. Philadelphia: W. B. Saunders Company, 1973.

Appendix A

Constants of the Aircraft Model

This appendix contains all the modelling constants used in the controller design simulation. The data represents a large fighter-bomber aircraft flying at sea level. The conditions for a standard atmospheric day are assumed.

Density $\rho = 2.378E-03 \text{ slug/ft}^3$

Speed of sound $A = 1116 \text{ ft/sec}$ (Ref 17:465)

Nominal aircraft velocity $V_o = 647.3 \text{ ft/sec}$ (Mach .58)

Aircraft weight $W = 55000 \text{ lbs}$

Wing area $S = 647 \text{ ft}^2$

Wing mean aerodynamic chord $\bar{c} = 18.678 \text{ ft}$

Dynamic pressure at nominal velocity

$$\bar{q} = \tfrac{1}{2} \rho V_o^2 S = 322307.6 \text{ slug-ft/sec}^2$$

Moment of inertia about aircraft y-axis

$$I_y = 380000 \text{ slug-ft/sec}^2$$

Appendix B

Stability Derivatives

This appendix presents all the stability derivatives in the controller design and explains their derivation. First of all, the dimensional stability derivatives are designated. Then the non-dimensional stability derivatives are explained. And, finally. the numerical values of all the stability derivatives are compiled.

Dimensional Stability Derivatives

The linear model in Chapter IV illustrated how the linearized equations of motion contain dimensional stability derivatives. These dimensional stability derivatives are the coefficients in the open loop dynamics matrix, Eq (27). These dimensional derivative values result from data computed by ASD/XRHA, Wright-Patterson AFB, Ohio. The definition of each dimensional derivative is included with its corresponding symbol. In addition, for dimensional derivatives required for further computation, the corresponding equation and units are included. The dimensional derivative equations and the units are compiled from Reference 16.

X_U, Dimensional Variation of x-force with Speed

$$X_v = \frac{-\bar{q}\, S\left(C_{D_v} + 2 C_{D_o}\right)}{m\, U_o} \quad (\text{sec}^{-1}) \qquad (B-1)$$

X_δ, Dimensional Variation of x-force with Elevator Deflection

$$X_\delta = \frac{-\bar{q}\, S\, C_{D_\delta}}{m} \quad (ft/sec^2) \qquad (B-2)$$

X_α, Dimensional Variation of x-force with Angle of Attack

$$X_\alpha = \frac{-\bar{q}\, S\left(C_{D_\alpha} - C_{L_o}\right)}{m} \quad (ft/sec^2) \qquad (B-3)$$

Z_U, Dimensional Variation of z-force with Speed

$$Z_u = \frac{-\bar{q}\, S\left(C_{L_u} + 2C_{L_o}\right)}{m\, U_o} \quad (sec^{-1}) \qquad (B-4)$$

Z_δ, Dimensional Variation of z-force with Elevator Deflection

$$Z_\delta = \frac{-\bar{q}\, S\, C_{L_\delta}}{m} \quad (ft/sec^2) \qquad (B-5)$$

Z_α, Dimensional Variation of z-force with Angle of Attack

$$Z_\alpha = \frac{-\bar{q}\, S\left(C_{L_\alpha} + C_{D_o}\right)}{m} \quad (ft/sec^2) \qquad (B-6)$$

M_U, Dimensional Variation of Pitching Moment with Speed

106

$$M_v = \frac{\bar{q} S \bar{c} \left(C_{m_v} + 2 C_{m_o} \right)}{I_y V_o} \quad \text{(ft-sec)}^{-1} \qquad \text{(B-7)}$$

M_δ, Dimensional Variation of Pitching Moment with Elevator

Deflection

$$M_\delta = \frac{\bar{q} S \bar{c} C_{m_\delta}}{I_y} \quad \text{(sec}^{-2}) \qquad \text{(B-8)}$$

M_α, Dimensional Variation of Pitching Moment with Angle

of Attack

$$M_\alpha = \frac{\bar{q} S \bar{c} C_{m_\alpha}}{I_y} \quad \text{(sec}^{-2}) \qquad \text{(B-9)}$$

The nine equations, Eq(B-1) through Eq (B-9), are required to compute the non-dimensional stability derivatives shown later in Appendix B.

It can be seen that the open loop dynamics matrix, A, in Eq (27) does not include the dimensional derivative terms X_α, Z_α, or M_α as coefficients. Instead, the longitudinal equations of motion include X_w, Z_w, and M_w respectively. With a simplified assumption these three variables in w can be transformed into variables in α for computation purposes. As seen in Fig. B-1 for small

107
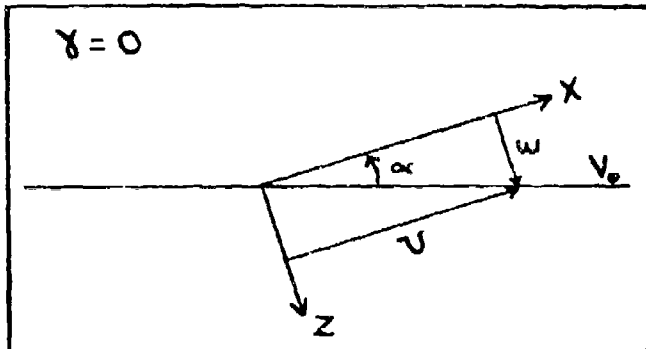
Figure B-1. Velocity Relationships

angles of attack, α, the following equation is true (Ref 12:72, 6:11)

$$\alpha = \frac{w}{V_o} \qquad (B-10)$$

There is also a relationship between dimensional stability derivatives as follows

$$X_\alpha \alpha = X_w w \qquad (B-11)$$

Substitution of Eq (B-10) into Eq (B-11) results in an important relation

$$X_w = \frac{X_\alpha}{V_o} \qquad (B-12)$$

Now, since the value of X_w is a known quantity from the open loop dynamics matrix, it is possible to solve for X_α

using Eq (B-12). There is an available equation, Eq (B-3), which is written in terms of X_α so it can be used to calculate the non-dimensional stability derivatives. The same process developed for X_α is used for the Z_α and the M_α equations. This is the method needed to solve for several unknowns in the nonlinear model equations.

Non-Dimensional Stability Derivatives

The non-dimensional stability derivatives are not used in the open loop dynamics matrix, A, but are required for the nonlinear model equations. The non-dimensional stability derivatives, with their definitions and pertinent equations, are listed below (Ref 16):

C_L is the lift coefficient

$$C_L = \frac{L}{\bar{q} S} \tag{B-13}$$

C_{L_α} is the aircraft lift curve

$$C_{L_\alpha} = \frac{\partial C_L}{\partial \alpha} \tag{B-14}$$

C_{L_δ} is the control surface lift effectiveness

$$C_{L_\delta} = \frac{\partial C_L}{\partial \delta} \tag{B-15}$$

C_{L_U} is the variation in lift coefficient with forward speed

$$C_{L_U} = \frac{\partial C_L}{\partial\left(\frac{U}{U_o}\right)} \qquad (B-16)$$

C_{L_o} is the lift coefficient for zero angle of attack.

C_D is the drag coefficient

$$C_D = \frac{D}{\bar{q}\,S} \qquad (B-17)$$

C_{D_α} is the variation in drag coefficient with angle of attack

$$C_{D_\alpha} = \frac{\partial C_D}{\partial\alpha} \qquad (B-18)$$

C_{D_δ} is the variation of drag coefficient with elevator deflection

$$C_{D_\delta} = \frac{\partial C_D}{\partial\delta} \qquad (B-19)$$

C_{D_U} is the variation of drag coefficient with forward speed

$$C_{D_U} = \frac{\partial C_D}{\partial\left(\frac{U}{U_o}\right)} \qquad (B-20)$$

C_{D_o} is the drag coefficient for zero angle of attack.

C_m is the pitching moment coefficient

$$C_m = \frac{M}{\frac{1}{2} S \bar{c}} \qquad \text{(B-21)}$$

C_{m_α} is the variation in pitching moment coefficient with angle of attack

$$C_{m_\alpha} = \frac{\partial C_m}{\partial \alpha} \qquad \text{(B-22)}$$

C_{m_δ} is the variation of pitching moment coefficient with elevator deflection

$$C_{m_\delta} = \frac{\partial C_m}{\partial \delta} \qquad \text{(B-23)}$$

C_{m_U} is the variation in pitching moment coefficient with forward speed

$$C_{m_U} = \frac{\partial C_m}{\partial \left(\frac{U}{U_o} \right)} \qquad \text{(B-24)}$$

C_{m_q} is the variation in pitching moment coefficient with pitch rate

$$C_{m_q} = \frac{\partial C_m}{\partial \left(\frac{q \bar{c}}{2 U_o} \right)} \qquad \text{(B-25)}$$

C_{m_o} is the pitching moment coefficient for zero angle of attack.

111

All of these non-dimensional stability derivatives
are required for the nonlinear model equations. The
numerical values are shown in the next section.

Stability Derivative Data

The values of the dimensional stability derivatives
are known from the open loop dynamics matrix, A (see
Chapter IV). From these known values and the model
constants all the necessary derivatives are calculated.
The actual dimensional stability derivatives are:

$$X_U = -.007578 \quad \text{sec}^{-1}$$

$$X_w = .01276 \quad \text{sec}^{-1}$$

$$X_q = .034 \quad \text{ft/sec}$$

$$X_\varsigma = -.000314 \quad \text{ft/sec}^2$$

$$X_\Delta = .000713 \quad \text{sec}^{-1}$$

$$Z_U = -.1029 \quad \text{sec}^{-1}$$

$$Z_w = -.8198 \quad \text{sec}^{-1}$$

$$Z_q = -2.175 \quad \text{ft/sec}$$

$$Z_\varsigma = -48.4 \quad \text{ft/sec}^2$$

$$Z_\Delta = -.0000361 \quad \text{sec}^{-1}$$

$$M_U = -.00013 \quad (\text{ft/sec})^{-1}$$

$$M_w = -.006086 \quad (\text{ft/sec})^{-1}$$

$$M_q = -.201 \quad \text{sec}^{-1}$$

$$M_\varsigma = -4.477 \quad \text{sec}^{-2}$$

Before the non-dimensional stability derivatives are
listed, the zero angle of attack conditions must be set.

These values are:

$$C_{L_O} = C_{m_O} = 0$$

$$C_{D_O} = .0106$$

With these zero angle of attack quantities, the remainder
of the stability derivatives may be calculated from the
equations of the first two sections of this Appendix.

$$C_L = .1706 \qquad\qquad C_{L_\zeta} = .2567$$

$$C_{L_\alpha} = 2.804 \qquad\qquad C_{L_U} = .35328$$

$$C_{D_\alpha} = -.0412 \qquad\qquad C_{D_U} = .00482$$

$$C_{D_\zeta} = 1.6654 \times 10^{-6} \qquad\qquad C_{m_\alpha} = -.2484$$

$$C_{m_U} = -.0053 \qquad\qquad C_{m_\zeta} = -.2326$$

$$C_{m_q} = -.8794$$

These values are used in the variety of equations in the
nonlinear controller model. This data is consistent with
actual flight test data (Ref 7 and 17).

Appendix C

Calculation of Trim Conditions

During the trim condition for stability the angular rates are zero, the linear rates are zero and, essentially, lift equals weight (Ref 7:30).

For the trim condition

$$L = \bar{q} S C_L = W \qquad (C-1)$$

Substitution of the known values into Eq (C-1) provides a value for C_L of

$$C_L = .1706$$

The corresponding C_L trim equation is

$$C_L = C_{L_\alpha} \alpha + C_{L_\delta} \delta \qquad (C-2)$$

Eq (C-2) is one equation needed to solve for the two trim angles, α and δ.

The pitching moment coefficient equation is written as

$$C_m = C_{m_0} + C_{m_\alpha} \alpha + C_{m_\delta} \delta \qquad (C-3)$$

For the trim condition $C_m = 0$ and Eq (C-3) becomes

$$0 = C_{m_0} + C_{m_\alpha} \alpha + C_{m_\delta} \delta \qquad (C-4)$$

From Appendix B the value of C_{m_o} is zero for the controller design, so Eq (C-4) reduces to

$$0 = C_{m_\alpha} \alpha + C_{m_\delta} \delta \qquad \text{(C-5)}$$

This is the second equation required to solve for the two unknown trim angles. Eq (C-2) and Eq (C-5) can be solved simultaneously to yield the trim conditions of

$$\alpha_{TRIM} = .0662 \text{ rad}$$

and

$$\delta_{TRIM} = -.0582 \text{ rad}$$

These two trim angles are used for calculations in the nonlinear reference model.

Appendix D

MOD6DF Computer Program

The Litton MOD6DF algorithm is a six-degree-of-freedom digital simulation program useful as a tool to analyze various guidance and control systems. It uses a modular approach to FORTRAN programming which allows the user flexibility to adapt modules to various physical systems. This appendix consists of a summary of the MOD6DF program. For more detail about the algorithm the reader should consult Reference 5.

Program Structure

The MOD6DF program is structured for systems engineers rather than programmers. It permits an engineer to use the overall program without being too concerned about numerous programming details. An engineer only needs to modify an independent module representing the physical system of interest.

The basic structure of the MOD6DF program is built around three main levels of subroutines (see Figure D-1). These three types of subroutines are:

    (a)   Type 0 - Executive subroutines which manage and supervise the overall MOD6DF program

    (b)   Type 1 - Operational subroutines which provide control at the beginning of each integration step
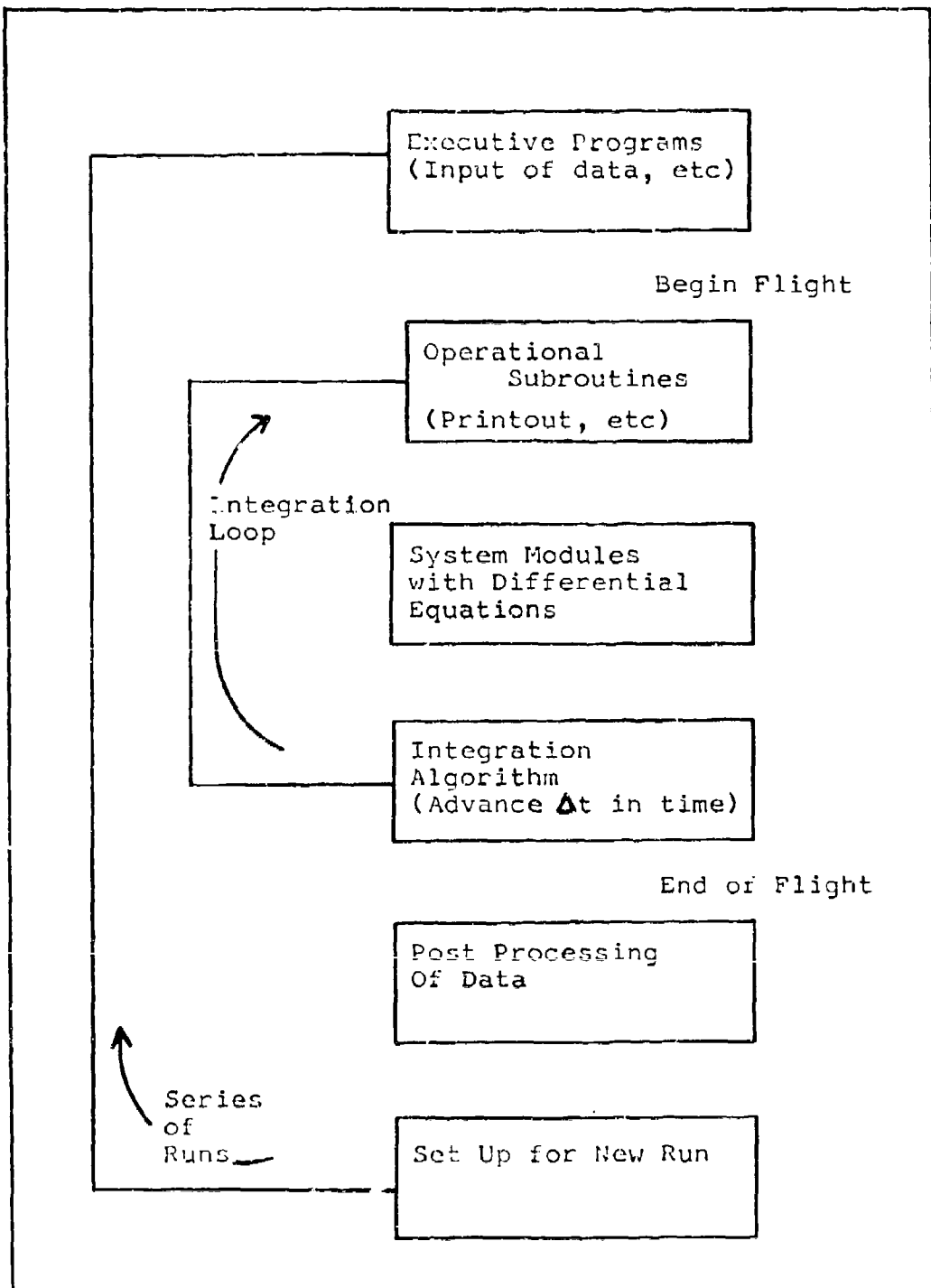
Figure D-? Structure of the MOD6DF Program (Ref 5:3)

(c)   Type 2 – Modules which are constructed by the
        user according to the physical system being
        investigated

The executive and operational subroutines are not
normally modified by the user. The modules are the
"black boxes" of the MOD6DF program which represent
modelling equations from the physical system. The proper
development of these modules is the main concern of an
engineer utilizing the MOD6DF program.

Operation

The MOD6DF program operates basically as an inte-
gration subroutine package. It utilizes a fourth-order
Runge Kutta integration scheme in closed form. Within
each module there is a number of differential equations
representing the physical system. The user identifies
the locations of the variables which are integrated
by writing certain specifications in an initialization
module. Using the integration algorithm, the system
solution progresses at each point in time by processing
the specified differential equations to advance the solu-
tion one step Δt in time. Computed values of various
variables may be stored at each step Δt for later use
as output data or for plotting. The program can also
generate random noise for Monte Carlo simulation and can
perform covariance simulation.

Most of the communication between subroutines is

118

accomplished through COMMON locations. Many of the
COMMON storage locations are specified (Ref 5:23), but
others are reserved for the variables in the system
modules. Therefore, the user does not have to use CALL
statements or argument lists when performing analysis.
The COMMON locations are arranged so that each variable
being integrated is associated with four consecutive
COMMON locations. The first location is for the deriva-
tive of the variable which is specified by the differential
equation in the system module. The second and third
locations were previously for the lower and upper bounds,
respectively, on the integration error of that variable;
but, these are no longer in use. And, the fourth loca-
tion is for the variable itself. Figure D-2 illustrates
an example of how this COMMON arrangement works for the

Variable	Value	COMMON location
$\dot{V}$	F/m	301
V	$\int F/m$	304

Figure D-2. COMMON locations for a typical integration
basic equation $F = m\dot{V}$

Input Cards

The input cards to MOD6DF are of ten types. These
input cards are closely related to the operational sub-
routines and the system modules. As a result, the input
cards essentially dictate how the MOD6DF program will be

119

implemented for any particular data run. There is a
basic format for the input cards which must be strictly
followed. The ten types of input cards are shown below.

Type	Input Description
1	Operational subroutines to be used
2	System modules to be used
3	Numerical input data including initial conditions
4	Variables to be printed out
5	Variables to be controlled
6	Parameters of random number generators
7	Variables to be plotted
8	Spare
9	Spare
10	Indicates end of a data run

Appendix E

The OPTSYS Program

This appendix explains the input and output para-
meters of the OPTSYS computer program. It does not
describe the program operation in detail since that is
the purpose of Reference 3.

Program Description

OPTSYS is a digital algorithm which utilizes optimal
control theory to calculate optimal gains for a system of
the general form

$$\delta \dot{\underline{x}} = A \delta \underline{x} + B \delta \underline{u} \tag{E-1}$$

using a cost function written as

$$J = \frac{1}{2} \int \left(\delta \underline{x}^T P \delta \underline{x} + \delta \underline{u}^T R \delta \underline{u} \right) dt \tag{E-2}$$

The OPTSYS program solves the steady-state form of
the matrix Ricatti equation to obtain the corresponding
Ricatti gain matrix, S. It is possible to compute the
feedback gain matrix, G, using

$$G = -R^{-1} B^T S \tag{E-3}$$

where all three matrices on the right hand side of

121

Eq (E-3) are known. The linear control law is

$$\delta \underline{u} = G \delta \underline{x} \qquad \text{(E-4)}$$

which permits substitution of Eq (E-4) into Eq (E-1) to yield

$$\delta \underline{\dot{x}} = (A + BG) \delta \underline{x} \qquad \text{(E-5)}$$

The resulting matrix, A+BG, is called the closed loop dynamics matrix. The stability characteristics of this closed loop matrix determines how well a feedback controller operates.

Input Parameters

OPTSYS requires the following parameters for operation:

(a) A the open loop dynamics matrix

(b) B the control distribution matrix

(c) P the state weighting matrix

(d) R the control weighting matrix

Using these four matrices which correspond to the standard form of Eqs (E-1) and (E-2), the optimal gains are calculated.

Output Parameters

The output quantities of the OPTSYS program are:

(a) the eigenvalues and eigenvectors of the open loop dynamics matrix, A

(b) the steady-state Ricatti gain matrix, S

(c) the feedback gain matrix, G

(d) the closed loop dynamics matrix, A+BC, and its associated eigenvalues and eigenvectors

Additional Uses

For the purpose of this thesis OPTSYS performed calculations as a deterministic controller. It is possible to introduce noise in OPTSYS and to perform stochastic calculations using estimation theory. Procedures for this mode of operation may be found in Reference 3.

VITA

Ronald Thomas Kelly was born on 29 July 1948 in Astoria, New York. He graduated from Floral Park Memorial High School in 1966 and entered the USAF Academy. Upon graduation in 1970 he received a Bachelor of Science in Aeronautical Engineering and was commissioned in the United States Air Force. He went on to navigator training at Mather AFB where he received his navigator wings in April 1971. Subsequently, he flew as a navigator on a C-130 at Forbes AFB and Kadena AB. He returned to Mather AFB in 1974 and served as a navigator instructor until entering the School of Engineering, Air Force Institute of Technology, in June 1976.

REPORT DOCUMENTATION PAGE		READ INSTRUCTIONS BEFORE COMPLETING FORM
1. REPORT NUMBER ✓ AFIT/GA/EE/77-3	2. GOVT ACCESSION NO.	3. RECIPIENT'S CATALOG NUMBER
4. TITLE (and Subtitle) Optimal Terrain Following Controller for an Optimized Spline Reference Path		5. TYPE OF REPORT & PERIOD COVERED MS Thesis
		6. PERFORMING ORG. REPORT NUMBER
7. AUTHOR(s) Ronald T. Kelly Capt USAF		8. CONTRACT OR GRANT NUMBER(s)
9. PERFORMING ORGANIZATION NAME AND ADDRESS (AFIT/EN) Air Force Institute of Technology Wright-Patterson AFB, Ohio 45433		10. PROGRAM ELEMENT, PROJECT, TASK AREA & WORK UNIT NUMBERS ASDP 0032 22600
11. CONTROLLING OFFICE NAME AND ADDRESS Deputy for Development Planning(ASD/XRHA) Aeronautical Systems Division Wright-Patterson AFB, Ohio 45433		12. REPORT DATE December 1977
		13. NUMBER OF PAGES 133
14. MONITORING AGENCY NAME & ADDRESS(if different from Controlling Office)		15. SECURITY CLASS. (of this report) UNCLAS
		15a. DECLASSIFICATION/ DOWNGRADING SCHEDULE

16. DISTRIBUTION STATEMENT (of this Report)

Approved for public release; distribution unlimited.

17. DISTRIBUTION STATEMENT (of the abstract entered in Block 20, if different from Report)

18. SUPPLEMENTARY NOTES

Approved for public release; IAW AFR 190-17

JERRAL F. GUESS, Captain, USAF
Director of Information

19. KEY WORDS (Continue on reverse side if necessary and identify by block number)

Terrain Following
Optimal Controller
Cubic Spline

20. ABSTRACT (Continue on reverse side if necessary and identify by block number)

This thesis presents the design of a proposed terrain
following flight controller capable of tracking a cubic spline
reference path. The controller tracks only the longitudinal
motion; however, it provides both thrust and elevator control.
The controller is based on a nonlinear reference model
constructed from an optimized spline path. The spline path
altitude and associated derivatives are computed. The longi-

DD $^{FORM}_{1 JAN 73}$ 1473   EDITION OF 1 NOV 65 IS OBSOLETE

tudinal equations of motion are linearized about the reference
trajectory and a truth model of actual aircraft motion is
developed. Deviations from the nonlinear reference trajectory
to the actual provide a linear system. Optimal control theory
is used to solve the resulting linear regulator problem. The
feedback gains are calculated from the steady-state Ricatti
matrix equation. The two system controls are updated using
these feedback gains.

Results show the feedback controller to be stable and
capable of tracking the cubic spline reference path. The per-
formance index weighting matrices can be adjusted to improve
the controller. The resulting controller can provide both good
path control and engine control to improve vehicle survivabili-
ty, engine life and fuel consumption.